

List of Major Changes

- Global changes: Revision of text structure according to readability and story line
- We changed the order of Sections 2 and 3;
- We changed the title of new Section 3 to “Data Sets” only (former “2. Data Sets and Methods”) and we shifted the method section 2.4 (3.4) “event definition and statistical distribution functions” into the model description (new Section 2.6) for better story line.
- We added Section 3.4 on numerical weather prediction models as used for further model validation in revised manuscript version (section 6).
- New Figure 2: Flowchart of model components with respective description in Section 2.1.
- New Section 4.3 “sensitivities of simulated precipitation” with new Figures 8 and 9.
- We added a paragraph in Section 5.1 on correlations of input variables.
- We removed the former Figure 11: We conclude that there is no added value of this Figure compared to Figure 10. Instead, we add more detailed analysis of model sensitivities (4.3).
- Section 6: We extend the model validation by statistics of stochastic simulations with the reduced SPM (basic model) and COSMO reanalysis data. The former Figure 12 was split into two new Figures (14 + 15) with the new corresponding sub-figures being added. We also added the related statistics to Figure 16a.
- We did adjustments to the Conclusions sections according to the points mentioned above; We also added a paragraph in the conclusions on the transferability of the presented method to different investigation areas.

Point-by-point response to Reviewer #1

Florian Ehmele on behalf of the co-author

July 09, 2018

Thank you very much for your work and the useful and valuable comments that helped to improve the scientific quality of our manuscript. Please find below our reply to the individual points.

This study extended the previous models from Smith and Barstad (2004) and Barstad and Smith (2005) to stochastically generate extreme precipitation events. The model relates extreme precipitation to atmospheric conditions, kind of circulation-based model. This model is exclusively for extreme precipitation events, different from those models for long-term weather generation. The paper presented a lot of details to interpret the procedures about development, calibration and validation of the proposed model. The topic falls within the scope of HESS.

Although the manuscript gave enough information about the model, it is not so easy to follow in the current form. I strongly suggest adjustments of the paper structure. First, a flowchart should be given to show the development, calibration and validation of the model.

We understand the reviewer's point that the manuscript may be difficult to follow. In the revised version of the manuscript, we try to improve the readability by re-organizing the sections and by tightening / deleting details that are not that important. We follow the suggestion and included a flow chart with corresponding descriptions in the text that may help to better understand the links among the different components.

Second, it is better to first give the model description following by data description, which is the usual way for method development.

In the new version of the manuscript, we changed the order of Sections 2 and 3 as suggested. We also rearrange some Sections to improve the logical story line.

Third, it is necessary to simplify some sections, but focus on how to connect atmospheric conditions with extreme precipitation so that the modeled data can represent the regional condition instead of one site.

Ambient conditions directly feedback into the model equations that combine flow conditions with microphysics, thus representing the regional conditions. This is highlighted, for example, in Figures 7 and 9 (which will be Figs. 8 and 10 in the revised version). Furthermore, to highlight directly the relation between environment and ambient conditions, we will include a new Figure. Another critical point is that we used only data from one radiosounding (Stuttgart). As shown by Kunz (2011) for a comparison between Stuttgart and Nancy sounding, ambient conditions during large-scale heavy rainfall usually do not show large gradients (at least for the parameters considered in the model and without fronts that are, thus, treated separately). We will add a comment in the manuscript.

Fourth, usually, for model development, a comparison with a paralleled model is necessary. Please consider the possibility to add this part. Although it takes time to do additional comparison, it is persuasive to highlight the strength of your model. Further, people would wonder how your model's performance compare with the

models for long-term weather generation. With the above adjustments, the manuscript would be easier for readers to understand.

We agree with the reviewer that a comparison with other models would be appropriate to highlight the skill and characteristics of our model. However, we are not aware of any comparable large-scale two-dimensional stochastic precipitation model. Therefore, we will compare the full SPM2D using the basic setup (reduced SPM; rSPM) with COSMO-CLM (CCLM) reanalysis using the top200 events. For this, we split Figure 12 into two new Figures 13 and 14, one for the median and one for the 90th percentile, and add the corresponding statistics of the rSPM and CCLM simulations. The same will apply to Figure 13 (new Fig. 15).

Furthermore, the authors should state the potential extension of the proposed models to the other regions in the world, which would be helpful for readers to know how to use it. Otherwise, it is a model just applicable to a specific region, which is not necessary to publish it in an international journal.

The methodology is not limited to a specific region. The basic core of the model, the orographic rainfall model according to Smith and Barstad (2004), has been applied successfully to several regions around the world (e.g., US, Norway, Iceland, Germany). Our extension, the stochastic approach, only requires precipitation totals to estimate background and frontal precipitation including calibration. We will add a comment about the potential transferability in the conclusion section.

References

Kunz, M.: Characteristics of Large-Scale Orographic Precipitation in a Linear Perspective, *J. Hydrometeorol.*, **12**, 27–44, 2011.

Smith, R. B. and Barstad, I.: A Linear Theory of Orographic Precipitation, *J. Atmos. Sci.*, **61**, 1377–1391, 2004.

Point-by-point response to Reviewer #2

Florian Ehmele on behalf of the co-author

July 09, 2018

Thank you very much for your work and the useful and valuable comments that helped to improve the scientific quality of our manuscript. Please find below our reply to the individual points.

This is a difficult paper to read – I think some rewriting and tightening would help exposition and the reader understand what the main contributions are.

We understand the reviewer's point that the manuscript may be difficult to follow. In the revised version of the manuscript, we try to improve the readability by reorganizing the sections and by tightening / deleting details that are not that important. We will also add a flow chart showing the different components of the model as suggested by Reviewer #1 to better understand the model's different components and their links.

In terms of the scientific problems, my major concerns can be summarized by the following comments:

1) How can you be sure the model isn't overfit? There are numerous parameters and features, and a seemingly exhaustive parameter estimation method is used, but shouldn't there be a cross-validation study where training data are used to fit the model, and held-out testing data are used to validate the goodness-of-fit?

We don't really see a conflict with overfit or "overengineering". All four components of the model (orographic, background, frontal, embedded-convection) are physically-based processes related to vertical lifting on different scales. The parameter estimation mainly is required for the dynamical core (wave dynamics) and the microphysics. For clarification, we will add a comment on this in the conclusion section. Considering the question of cross-validation, we fully agree. However, this was already done. The model is trained for a set of approx. 100 events and then driven stochastically over 10.000 events. The stochastic simulations, the main purpose of the model, are evaluated against the observations using different statistical quantities. To avoid any confusion, we will highlight this in the manuscript.

2) Lack of comparison against a simpler model. There are many moving pieces in this model; which components are giving the most improvement? In particular, it would be helpful to consider simpler versions of the model and compare their relative performance in simulation, this would help the reader understand which contributions are the most important and where future research may focus.

We agree that adding a comparison to simpler versions or to other models would highlight the potential and skill of our approach (this point was also recommended by reviewer #1). As to the best of our knowledge there is no comparable stochastic model available, we will use COSMO-CLM reanalysis instead, but focusing on historic events. We will split the four-part Figure 12 into two Figures (new 13 and 14), one for the median and one for the 90th percentile and add the corresponding statistics for both cases using the reduced stochastic model (rSPM, basic model) and reanalysis data performed with the COSMO-CLM model. We same will apply for Figure 13 (new Fig. 15). With those additions the improvements of the model should become clearer.

3) How well are spatial correlations maintained in the model? Spatially aggregated statistics like max, min and means are validated, but what about raw correlations?

We are not sure what the reviewer exactly means with “raw correlations”. The presented analysis of maximum and minimum values in Figure 13 is not spatially aggregated, but show max/min values at each grid point in the model domain. The median and percentile values presented in Figure 12 as well as the difference between model and observations for different return periods shown in Figure 14 are grid point-based statistics and not spatially aggregated. As the SPM is event-based and not designed for continuous simulations of extreme events it is not possible to correlate “time series” between simulations and observations for the different grid points. Considering wave dynamics in combination with an FFT algorithm, a spatial conjunction is already given.

Point-by-point response to Reviewer #3

Florian Ehmele on behalf of the co-author

July 09, 2018

Thank you very much for your work and the useful and valuable comments that helped to improve the scientific quality of our manuscript. Please find below our reply to the individual points.

The authors have taken a physically-based, simplified model of orographic precipitation and added mitigations in their approach. The approach has been tested with good results.

It is an interesting and valuable contribution to the literature on this subject. It is thoroughly done and, given the complexity of the approach, it is easy to follow. I would say the results are convincing and robust. Below is a few comments/questions.

Main question: It seems to me that the input parameters are treated independently, section 5.1, in this approach. We know that input parameters such as wind speed and direction are not independent, and thus should not be treated as such. Categorization helps, but still leaves us with the problem mentioned above. If I have understood this correctly, how do you justify independence (picking from pdf's in a random fashion)?

This is a very helpful comment. To address this point, we will add a new section "4.3 Model sensitivities" to the paper with a more detailed sensitivity study of total precipitation to varying initial conditions including discussion in Section 5.1. Our results show different behaviors of the correlations between the input variables. Overall, the relation between the input parameters is weak with correlation coefficients in most cases between +/- 0.3, and only for two parameters of +/- 0.7. After seasonal differentiation, there are significant correlations in only one season. Those cases with higher correlation are mainly related to stability (saturated Brunt-Väisälä frequency N_m^2). As shown in Figures 7 and 9, however, the model is less sensitive to this parameter compared to other. Taking into account the three points mentioned above, we found it acceptable to treat the input variables independently to keep the SPM as simple as possible. We will add a statement on this.

Minor comments/questions:

P7, L12, "linear model assumes penetration through the whole atmosphere...": Does it? it is contrary to what you write below Eq. 6, L24 which I thought was the idea of wave dynamics; reduced penetration with height. Perhaps the over-estimation has something to do with the saturation assumption you mentioned?

This was incorrect as wave dynamics show vertically tilted waves that also decay with height (expect when $Fr = U/NH$ is very large and where the solution more or less resembles the simple upslope approach). Furthermore, you are right that the assumption of saturation over all atmospheric layers, where also the lifting condensation level is at the surface, may lead to an overestimation of modelled precipitation. We will correct/change this in the text.

P9: If c_{oro} is constant in the whole domain, it could be enter in wave space. Can it be collapsed with f_{Cw} into a common factor, reducing the number of free parameters?

This might be possible. However, these two parameters affect different physical processes. f_{Cw} acts to reduce the uplift sensitivity of the model; therefore, it mostly affects areas with strong gradients in orography (compare Figure 2), whereas over less gradients with less orographic lifting the effect is weak. Additionally, multiple ascends/descents are possible without changes in water vapor content of the air parcel. Even though c_{oro} has the same effect, this parameter is independent from any lifting process and is applied throughout the domain. As mentioned in the text, it is a consequence of the assumption that vertical lifting of the entire column of air leads to condensation and instantaneous fallout of hydrometeors at any time. To deal with the resulting overestimation of available precipitable water, c_{oro} was implemented. We will change the text to better understand this point.

Fig 15: I believe that the confidence interval should be wider on the upper side than the lower side (due to fewer data points).

Yes, you are right. After checking the data and the routine, we conclude that the used empirical formula from Dyck (1980) is not the proper way. We redid the plots of Figure 15 (old numbering) using the statistical calculation described by Maity (2018) and replaced it in the new manuscript version.

References

Dyck, S., 1980: Angewandte Hydrologie, Teil 1: Berechnung und Regelung des Durchflusses der Flüsse., 2 edn.

Maity, R., 2018: Statistical Methods in Hydrology and Hydroclimatology, Springer Nature Singapore Pte Ltd., <https://doi.org/10.1007/978-981-10-8779-0>, 2018.

Flood-Related Extreme Precipitation in Southwestern Germany: Development of a Two-Dimensional Stochastic Precipitation Model

Florian Ehmele¹ and Michael Kunz^{1,2}

¹Institute of Meteorology and Climate Research, Karlsruhe Institute of Technology (KIT), Hermann-von-Helmholtz-Platz 1, 76344 Eggenstein-Leopoldshafen, Germany.

²Center for Disaster Management and Risk Reduction Technology (CEDIM), KIT - Karlsruhe, Germany

Correspondence to: Florian Ehmele (florian.ehmele@kit.edu)

Abstract. Various application fields, such as insurance industry risk assessments for the design of flood protection systems, require reliable precipitation statistics in high spatial resolution, including estimates for events with high return periods. Observations from point stations, however, lack ~~of~~ spatial representativeness, especially over complex terrain, ~~and~~. Thus, they do not reliably represent the heavy tail of the distribution function. Common numerical weather models are not capable of
5 running simulations over thousands of years. This paper presents a new ~~method for stochastically simulating precipitation fields~~
numerical method to simulate larger-scale precipitation fields stochastically, based on a linear theory ~~of describing~~ orographic
precipitation and additional functions that consider synoptically driven rainfall and embedded convection in a simplified way. The model is initialized by various statistical distribution functions describing prevailing atmospheric conditions, such as wind
vector, moisture content, or stability, estimated from radiosonde observations for a limited sample of the 200 strongest rainfall
10 events observed.

The model is applied for the stochastic simulation of heavy rainfall over the complex terrain of Southwest Germany. It is shown that the model, despite its simplicity, yields reliable precipitation fields. Differences between observed and simulated rainfall statistics are small, being in the order of only $\pm 10\%$ for return periods of up to 1,000 years.

1 Introduction

15 Persistent precipitation over large areas and the resulting widespread flooding frequently cause major damage in Central Europe in the order of several billion ~~EUR~~Euro (EUR) per event. In Germany, two extreme floods in 2002 and 2013 with estimated return periods of more than 200 years (Schröter et al., 2015) collectively caused more than EUR 22 billion in economic losses (inflation adjusted to 2017; MunichRe, 2017). ~~Besides~~Beside these extreme events, smaller floods with higher frequencies, such as those in ~~the years of~~ 2005, 2006, 2010, and 2011 (Uhlemann et al., 2010; Kienzler et al., 2015), also contribute to the
20 large damage potential associated with floods.

Flood risk estimation, for example, for insurance purposes or for the design of appropriate flood mitigation systems, requires the ~~reliable~~dependable statistical analysis of extreme rainfall. Traditionally, these extremes have been estimated at point stations from intensity-duration-frequency (IDF) with extreme value statistics being applied (Koutsoyiannis et al., 1998). This method, however, implies two ~~eaveats~~drawbacks: (i) the low spatial representativeness of point observations and (ii)

the limited observation period so that not all possible extreme configurations enter the samples. To account for the former ~~point~~shortcoming, either geostatistical interpolation routines, such as kriging (Goovaerts, 2000), or techniques that relate precipitation to both orographic characteristics and atmospheric parameters (e.g., Basist et al., 1994; Drogue et al., 2002) are ~~applied~~used. Shortcomings resulting from these methods are the lack of representativeness of station data with respect to the surroundings, and the neglect of dynamical and thermodynamical processes decisive for real precipitation events. To account for the limited observation period, several studies have employed stochastic weather generators to simulate precipitation events at single grid points (e. g., Richardson, 1981; Furrer and Katz, 2007; Neykov et al., 2014). A recent study by Cross et al. (2017) introduced a censored rainfall modeling approach designed to reduce the underestimation of extremes. Albeit considering the long-term variability of precipitation, which leads to more reliable estimates for extremes, these approaches still lack ~~of~~ spatial representativeness.

In the present study, we ~~propose~~present a two-dimensional stochastic precipitation model (SPM2D) that allows for simulating a large number of precipitation fields ~~with~~using a high spatial resolution. Large sample sizes of several thousand events are required to obtain ~~reliable and~~ robust estimates of the hazard for high recurrence periods, ~~such as~~like the one-in-200-year events that have to be considered by insurance companies. Common numerical weather models are not capable of simulating thousands of years due to their complexity and the resulting long computation time.

The core of our SPM2D is the diagnostic linear model approach for orographic precipitation according to Smith and Barstad (2004). The model considers wave dynamics in terms of the linearized equations of a stratified, non-hydrostatic flow over mountains (Smith, 1980). Input parameters are atmospheric flow quantities connected to precipitation, such as stability, moisture scaling height, precipitable water, or flow speed, all estimated from radiosoundings. Additional internal free parameters, such as characteristic time scales for cloud water conversion and fallout, serve as calibration parameters. The Smith and Barstad (2004) model has been successfully applied in various regions, ~~such as~~e. g. several locations in the United States (Barstad and Smith, 2005), Iceland (Crochet et al., 2007), Southwest Germany (Kunz, 2011), or Southern and Northern Norway (Caroletti and Barstad, 2010; Barstad and Caroletti, 2013). ~~It is found that despite~~ Despite the fact that characteristic time scales and background precipitation may vary from one situation to another, it is found that simulations using fixed values for the free parameters yield ~~reliable and robust~~trustworthy results. In our approach, we added two additional components to the orographic and background precipitation: synoptic-scale fronts and convection embedded into mainly stratiform clouds (Fuhrer and Schär, 2005). Whereas the former component may enhance (or reduce in case of absence) precipitation over larger areas, the latter may lead to ~~slightly locally~~locally slightly enhanced totals.

In the present study, we applied the SPM2D to both single historical events with heavy rainfall (training events) and over a long-term period of several thousand years (~~events~~over Southwest Germany (Fig. 1), validation events). In the latter case, the required model parameters are estimated from probability density functions (~~pdf~~pdfs) and are stochastically ~~simulated~~selected. In this application, we fixed the internal free parameters to constant values estimated by thorough calibration. ~~Due to varying~~ Because precipitation regimes in summer and winter vary significantly, we seasonally differentiate our analyses.

The investigation area for this study is the Federal State of Baden-Württemberg (BW) in Southwest Germany, which extends from 46.6 to 50.8° N and from 6.9 to 11.1° E (Fig. 1). The terrain exhibits a certain degree of complexity: with the broad Rhine

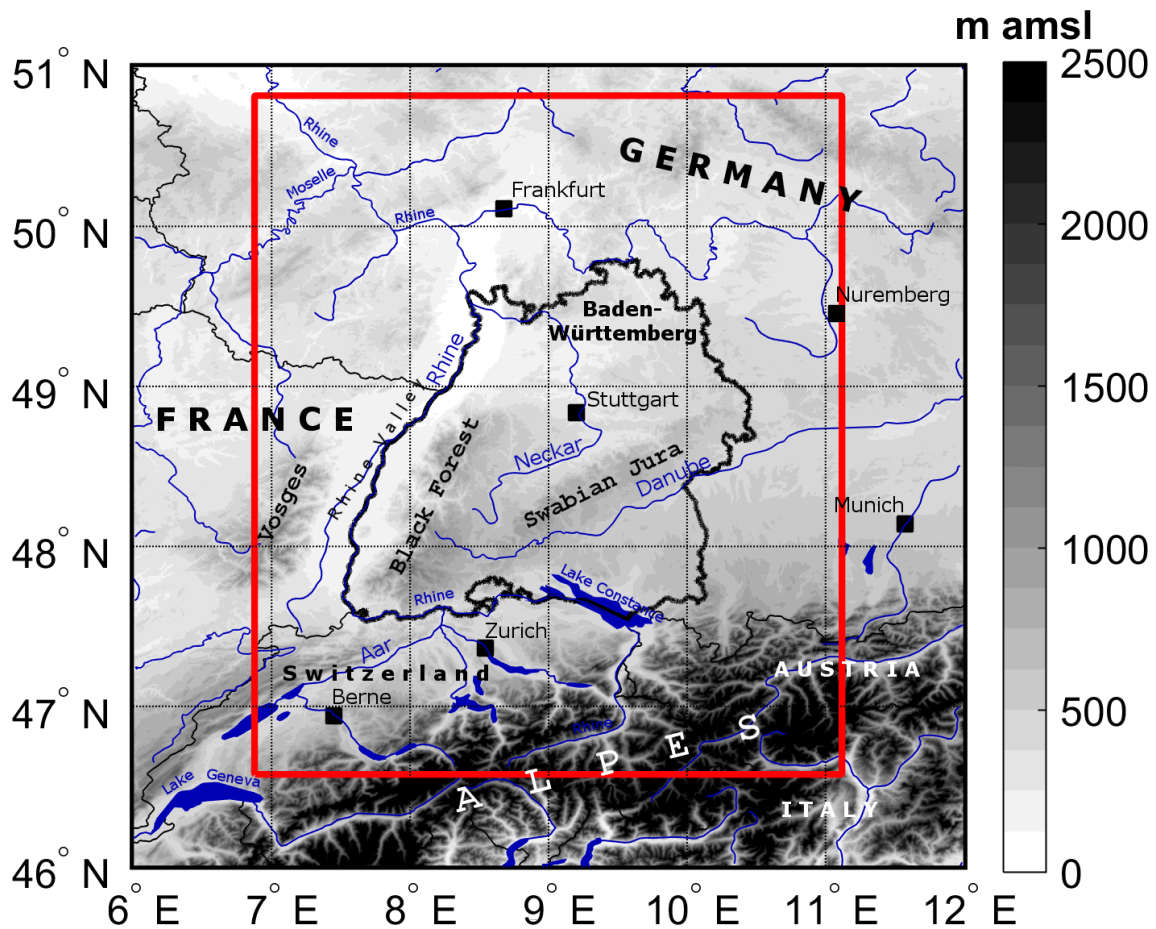


Figure 1. Topographic map of Southwestern Germany and surrounding areas with main river networks and lakes as well as substantial orographic structures; The national borders (slim solid black contours) and the border of the Federal State of Baden-Württemberg (bold solid black contour) are shown as well as the model domain (red box).

Valley with elevations of 100–200 m bounded by the Vosges Mountains (France) to the west and the Black Forest mountains to the east; with a maximum elevation of 1493 m (Feldberg) in Southern Black Forest; and with some rolling terrain to the northeast. Annual precipitation is between 600 mm (southern Rhine Valley) and approximately 2000 mm (southern Black Forest).

5 The presented SPM2D is one component of a risk assessment methodology that estimates the risk for a local direct insurer by quantifying the maximum probable loss for a 200-year return period (PML200). The other risk assessment components, however, are not further discussed in this paper.

The paper is structured as follows: Section 2 ~~briefly describes the data sets used in this study~~introduces the basics of the SPM2D. Section 3 ~~introduces the basics of the SPM2D~~briefly describes the data sets used in this study. Section 4 presents

the results of the calibration based on a set of 200 historical heavy rainfall events; and [gives a sensitivity study of the model depending on varying ambient conditions](#). Section 5 shows some characteristics of the selected events. [Simulation results](#) [Results of the stochastic simulations](#) are discussed in Section 6, and Section 7 lists some conclusions.

2 Data and methods

5 The SPM2D presented in this study is based on two different data sets: gridded precipitation data to estimate background precipitation and to calibrate and verify the model, and vertical profiles from radiosondes to initialize the model. Unless otherwise indicated, the investigation period covers the years of 1951–2016 (hereinafter referred to as IP). The investigation area is the Federal State of Baden-Württemberg (BW) in Southwest Germany, which extends from 46.6 to 50.8° N and from 6.9 to 11.1° E (Fig. 1). The terrain exhibits a certain complexity with the broad Rhine Valley; with elevations of 100–200 m
10 bounded by the Vosges Mountains (France) to the west and the Black Forest mountains to the east; with a maximum elevation of 1493 m (Feldberg); and with some rolling terrain to the northeast. Annual precipitation is between 600 (southern Rhine Valley) and approximately 2000 mm (southern Black Forest).

2.1 Rainfall totals

Rainfall statistics in our study are based on the REGNIE (*REGionalisierte NIEderschläge*, regionalized precipitation) data
15 set provided by the German Weather Service (Deutscher Wetterdienst; DWD). REGNIE is a gridded data set of 24-hour totals based on several thousand climate stations more or less evenly distributed across Germany (so-called RR collective). The REGNIE algorithm interpolates the observations to a regular grid considering elevation, exposition, and climatology (Rauthe et al., 2013). The REGNIE area contains 611 grid points in the west–east direction with $5.83^\circ \text{ E} \leq \phi \leq 16^\circ \text{ E}$ and 971 grid points in the north–south direction with $47^\circ \text{ N} \leq \theta \leq 55.08^\circ \text{ N}$ (ϕ : longitude; θ : latitude). Grid points outside of Germany
20 are set to malfunction. The spatial resolution of REGNIE is approximately 1 km², and the observation period is from 06 to 06 UTC.

It should be noted that REGNIE data are temporally not homogeneous due to changes in the locations and number of rain gauges. Furthermore, because the number of stations considered by the regionalization is limited, especially over elevated terrain, such as the Black Forest mountains, areal precipitation exhibits a certain bias. Its magnitude, however, cannot be
25 directly estimated from the observations solely (Kunz, 2011).

2.2 Radiosoundings

Input of the SPM2D are several atmospheric parameters derived from radiosoundings: thermal stability in terms of saturated Brunt-Väisälä frequency N_m (e. g., Lalas and Einaudi, 1973) and actual and saturated vertical temperature gradients (γ and Γ_m), water vapor scaling height H_w , water vapor mixing ratio q_v , wind speed U , and direction β (see Sect. 2). These parameters
30 are computed from the vertical profiles of temperature, moisture, wind speed, and direction at the radiosounding station of Stuttgart (48.83° N 9.20° E) located somewhat downstream of the northern Black Forest mountains. Even though the location

might not be ideal because the profiles do not represent undisturbed conditions, the profiles in the mean are similar to that of the upstream station of Nancy in France as shown by Kunz (2011). Data from Nancy, however are available after 1990 only and, thus, cannot be used in this study, whereas soundings from Stuttgart are available since 1957. In this study, we used the soundings at the main standard times for synoptic observations of 00 and 12 UTC.

5 Sounding data were provided by the Integrated Global Radiosonde Archive (IGRA) for quality-controlled radiosonde and pilot balloon observations from the National Climatic Data Center (Durre et al., 2006). These data at both main pressure levels and significant levels, where one of the parameters show a significant change, were interpolated into equidistant increments of $\Delta z = 10$ m (Mohr and Kunz, 2013). All parameters derived from the soundings refer to the lowest 5 km of the atmosphere since this layer is most relevant for air flow and stability. Furthermore, to account for the decreasing impact of higher atmospheric
 10 layers on the flow characteristics, all flow parameters Λ have been vertically integrated ($\tilde{\Lambda}$), with water vapor weighting being applied (Kunz, 2011):

$$\tilde{\Lambda} = \frac{\int_{z=0}^{z_t} \Lambda \rho_d q_v dz}{\int_{z=0}^{z_t} \rho_d q_v dz},$$

where ρ_d is the density of dry air and $z_t = 5000$ m.

As some layers may be moist-unstable, resulting in imaginary N_m , the averaging routine is applied to N_m^2 . In the few cases
 15 where \tilde{N}_m was imaginary, it was set to a near-neutral, constant value of 0.0003 s^{-1} .

2.3 Parameters for Embedded Convection

Embedded convection in the SPM2D is considered by single streaks of enhanced precipitation (see Sect. 2). These streaks are stochastically generated according to the statistical distributions of the observed maximum length L and width W of severe convective storms estimated by ??. In that study, convective storms were identified from the constant altitude plan position indicator (CAPPI) for a reflectivity in excess of 55 dBZ, also known as the Mason (1971) criterion for hail detection. The
 20 application of a tracking algorithm based on the concept of the algorithm of TRACE3D (Handwerker, 2002) yields entire tracks of convective storms. In total, more than 20,000 tracks over Germany, France, Belgium, and Luxembourg were identified during the summer half years (April to September) in the period 2004–2014. Even though we do not consider rainfall related to severe convective storms or hail in the SPM2D, the statistical distributions of the storm's dimensions are reliable proxies for
 25 the extension of enhanced precipitation from embedded convection.

2.4 Event definition and statistical distribution functions

Stochastic modeling of precipitation events with SPM2D requires the adjustment of appropriate probability density functions (pdf) to all input parameters. These pdfs are estimated from an appropriate set of past heavy rainfall events. Based on the pdfs, several thousands events can be stochastically generated (more details are found in Sect. 4). Because the characteristics of the
 30 ambient conditions and thus the precipitation regimes change throughout the year, we seasonally differentiate the estimated pdfs among spring (MAM), summer (JJA), autumn (SON), and winter (DJF).

In the first step, a sufficient and appropriate subset of relevant historic events was identified. An event here is defined as a period of one or more days with persisting precipitation above a certain threshold. Because our study focuses on major large-scale flood events and not on local-scale floods or flash floods, an extension to multi-day events is necessary. In this way, time delays in discharge response or flood waves traveling along river networks are implicitly considered (e.g., Duckstein et al., 1993; Uhlemann et al., 2010; Schröter et al., 2015).

We define the historic event set based on maximum areal precipitation. For this, we simply accumulate the (equidistant) 24-hour REGNIE-totals \bar{R}_{BW} of all grid points in BW. Following the sorting of all values of \bar{R}_{BW} in descending order, the strongest 200 values enter the sample (top200). As precipitation is not limited to these (single) days but may be embedded in longer time periods, we define the threshold of R_{thres} for event definition. Estimating R_{thres} , we consider “wet” days by using $\bar{R}_{BW} > 0$ solely, and we set R_{thres} to the 75% percentile of this sample. A lower threshold leads to an over-interpretation of longer clusters, a higher one avoids multi-day events.

Event precipitation starts on the first day that exceeds R_{thres} . When areal means of consecutive days are also above R_{thres} , they are simply accumulated, yielding events of more than one day. To ensure statistical independence, at least three days of non-exceedance have to prevail between two events in accordance with the approach of Palutikov et al. (1999) for wind storms. On the day that R_{thres} is not exceeded for the next three days as well defines the end of an event. In accordance with Piper et al. (2016), we solely count “rain days” ($\bar{R}_{BW} \geq R_{thres}$) and neglect “skip days” ($\bar{R}_{BW} < R_{thres}$) for event duration estimation, which is a widely used approach (Wanner et al., 1997; Petrow et al., 2009). This approach avoids the over-interpretation of longer clusters.

Based on the procedure described above, a defined precipitation event contains one or more days of the top200 sample. In the next step, we identified the pdfs most appropriate for statistically describing each of the seven model parameters. In total, 17 different pdfs were tested and compared with the distribution functions of each parameter for each of the four seasons (Table 1). In addition to 20 pdfs preset by the MATLAB statistic toolbox (MATLAB, 2016), we considered the circular von-Mises distribution (Mardia and Zemroch, 1975) for wind direction only. Note that Gumbel (GbD) and Weibull (WbD) distributions are special cases of the generalized extreme value distribution (GEV) and that some pdfs cannot be used for every parameter due to their ranges of validity.

To estimate the pdf that best fits the data, we estimated the appropriate number of histogram classes according to Freedman and Diaconis (1981), and we calculated the bias, root mean square error (rmse) and Spearman correlation coefficient r_{SP} (Spearman, 1904) as quality indicators (QIs). We also applied a χ^2 -test according to Wilks (2006) as a QI. For each QI, we ranked the pdfs in ascending order and added up the rank numbers for each pdf receiving the best fit in terms of the least QI-rank sum (QIRS). In the case of the alikeness of two or more pdfs (about 10% of all cases), we manually selected the best one.

2 Stochastic Precipitation Model

2.1 General description

The SPM2D, designed for widespread precipitation from essentially stratiform clouds, quantifies total precipitation R_{tot} from the linear superposition of four processes and terms:

$$R_{\text{tot}} = R_{\text{oro}} + R_{\infty} + R_{\text{front}} + R_{\text{conv}}. \quad (1)$$

R_{oro} estimates orographic rain enhancement, representing the central core of the SPM2D for complex terrain, ~~such as as for~~ instance those in BW. R_{∞} is the background precipitation related to large-scale lifting. These two parts originate from the linear orographic precipitation model of Smith and Barstad (2004) and Barstad and Smith (2005) with a few modifications, hereinafter referred to as reduced SPM2D (rSPM). In an extension of the rSPM, we included two additional precipitation components: R_{front} to account for precipitation related to synoptic fronts, and R_{conv} to consider embedded convection atop mainly stratiform clouds (e.g., Fuhrer and Schär, 2005; Kirshbaum and Smith, 2008). These two components were included because ~~linear theory assumes waves that penetrate through the whole atmosphere, leading to an overestimation of precipitation totals, whereas the related processes significantly contribute to the total precipitation amount and linear theory,~~ low intensities are underestimated tends to an underestimation of low intensities (e.g., Kunz, 2011).

The SPM2D ~~presented in this paper~~ is an event-based model. Instead of simulating continuous long-term periods of several years, a specific number n_{E} of independent events with various ~~durations~~ duration t_{ev} occurring during different seasons is simulated. The individual components are discussed more detailed in the following Sections. Starting the iteration loop over n_{E} events, first, the characteristics season and duration t_{ev} are allocated to the event (Fig. 2). Next step is the computation of the precipitation fields within the loop over t_{ev} . The components of the total precipitation in Eq. (1) are separated into two types: R_{oro} and R_{∞} are simulated 12-hourly (2 times a day), while R_{front} and R_{conv} are calculated 24-hourly (once a day). The linkage between the precipitation components and the corresponding input variables (pdfs; parameters) is also shown in Fig. 2. Note that the internal free model parameters are set to constant values for the entire simulation (illustrated as shaded box). After each 24-hour period, the total precipitation R_{tot} sums up according Eq. (1). In case t_{ev} is reached, the computation goes on to the next event until n_{E} events have been simulated.

Since the purpose of the model is to stochastically simulate a large number of several thousands events, the results can be used to robustly estimate rare events, such as the one-in-200-year events that the insurance industry must consider (probable maximum loss, PML200). The prerequisite, however, is a ~~reliable~~ decent simulation of single events.

2.2 Orographic precipitation

The linear precipitation model of Smith and Barstad (2004) and Barstad and Smith (2005), which is briefly described in this subsection, is a simple yet efficient way to compute precipitation over complex terrain. A total number of only seven atmospheric parameters estimated from sounding data (see Sect. 3.2) ~~are is~~ required to run the model. It is based on the three-dimensional (3D) linear flow according to Smith (1980) and Smith (1989). Thus, it explicitly considers linear flow effects

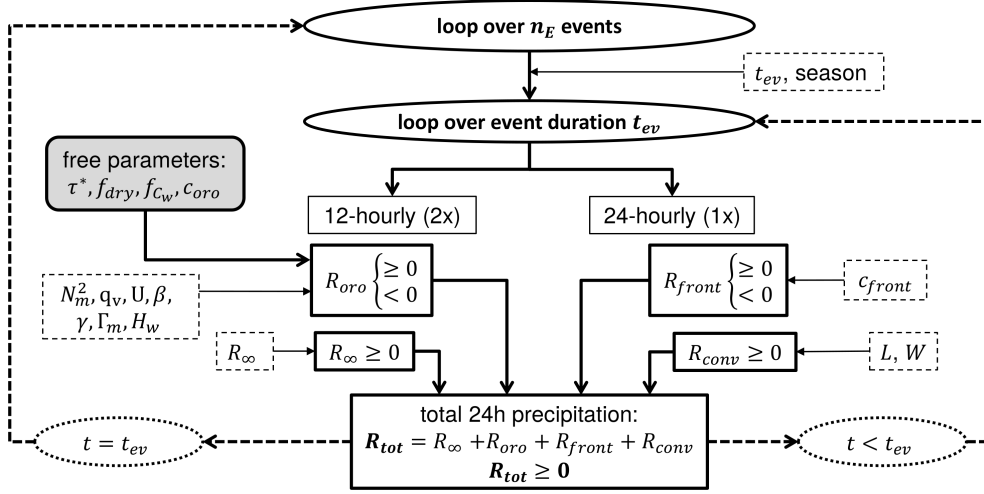


Figure 2. Flow chart of the individual components within the SPM2D (solid boxes) and the corresponding input variables (pdfs; dashed boxes). Iteration loops are highlighted as ellipsis or bold dashed arrows. The constant model parameters are illustrated as shaded box.

evolving over mountains, such as upstream-tilted gravity waves or flow that goes around rather than over an obstacle in the case of low wind speed, high static stability, and/or large mountains (i. e. small Froude numbers). It is assumed that saturated lifting produces condensed water that falls to the ground after a certain time shift (Jiang and Smith, 2003). Thus, precipitation on the ground is directly related to the condensation rate.

- 5 One of the key components of the linear model is a pair of linear steady-state equations for the advection of vertically integrated cloud water and hydrometeor density, q_c and q_h , during characteristic time scales:

$$\mathbf{v} \cdot \nabla q_c = S(x, y) - \frac{q_c}{\tau_c}, \quad (2)$$

$$\mathbf{v} \cdot \nabla q_h = \frac{q_c}{\tau_c} - \frac{q_h}{\tau_f}, \quad (3)$$

where τ_c and τ_f are time scales for cloud water conversion and the fallout of hydrometeors respectively. Both time scales are mathematically analogous and are assumed to be constant in time and space. When the time scales are set to zero, the maximum precipitation is almost one order of magnitude larger compared with a configuration with, for example, $\tau_f = \tau_c = 1000$ s (Kunz, 2011). Source-The source term S describes the mass flux of precipitation caused by orographic lifting. For positive S , ~~term~~ $q_c \tau_c^{-1}$ acts as a source in Eq. (3) and as a sink in Eq. (2). This term is proportional to the cloud water density integrated vertically from the bottom to the top of the lifting area. In light of this fact, it is assumed that the whole column is saturated in the case of lifting. The loss of hydrometeors, $q_h \tau_f^{-1}$ in Eq. (3), ~~determines precipitation rate R and~~ is proportional to the hydrometeor column density and determines the precipitation rate R . However, in the case of descending air with negative S downstream of mountains, evaporation occurs, and R may become negative.

A powerful method for ~~solving the~~ the solution of the advection equations for cloud physics, Eq. (2) and (3), together with the linear theory for 3D flow is to apply a two-dimensional (2D) Fourier transform. In ~~the~~ Fourier space, the precipitation rate $\hat{R}(k, l)$ is given by the following transfer function:

$$\hat{R}(k, l) = \frac{iC_w \sigma \hat{h}(k, l)}{(1 - imH_w)(1 + i\sigma\tau_c)(1 + i\sigma\tau_f)}, \quad (4)$$

5 which ~~relates-connects~~ the precipitation field in ~~the~~ Fourier space, $\hat{R}(k, l)$, ~~and-to~~ the orography, $\hat{h}(k, l)$, ~~with-both-related-to~~ the horizontal wavenumbers (k, l) . In ~~Equation~~ Eq. (4), i is the imaginary unit, and $C_w = \rho_{S_{ref}} \Gamma_m \gamma^{-1}$ is the uplift sensitivity related to condensation rate $\rho_{S_{ref}} = \rho_d q_v$, where ρ_d is the density of dry air ~~and-~~ q_v the water vapor density, and ~~where~~ Γ_m and γ are the moist adiabatic and actual lapse rates respectively. Water vapor scale height H_w is the height above ground where the vertical integrated horizontal water vapor flux has reached e^{-1} of its ground value. $\sigma = Uk + Vl$ is defined as the intrinsic
10 frequency with components U and V of the undisturbed horizontal wind vector that is assumed to be constant through time and space.

Whereas the nominator of Eq. (4) gives the dependency of precipitation on vertical motion and orography, the first bracket of the denominator describes the relation of the source term to airflow dynamics. The second and third terms of the denominator consider the advection of hydrometeors during characteristic time scales τ_x ($x = c; f$) and ~~-~~ evaporation in the case of descent;
15 evaporation.

Vertical wavenumber m in Eq. (4) is given by the dispersion relation (Smith, 1980):

$$m(k, l) = \left[\frac{N_m^2 - \sigma^2}{\sigma^2} (k^2 + l^2) \right]^{0.5}. \quad (5)$$

In this formulation, m controls both the depth and tilt of forced ascent or descent. Because vertical lifting is assumed to be saturated throughout the whole column, meaning that the lifted condensation level is located at the ground, saturated Brunt-
20 Väisälä frequency N_m has to be considered instead of the dry one, N_d . Compared with unsaturated flow, saturated flow leads to a weakening of the amplitude of ~~the~~ gravity waves via the reduction of static stability and thus to a flow that goes streaming more directly over the mountains rather than around as shown, for example, by Durran and Klemp (1982) or Kunz and Wassermann (2011). Even though the concept of saturated flow by simply considering N_m must be regarded as an approximation of the reality, it has been successfully applied by several authors studying flow dynamics and precipitation (Jiang and Smith, 2003;
25 Smith and Barstad, 2004; Kunz and Wassermann, 2011).

The precipitation field on the ground is obtained via an inverse Fourier transform of the transfer function Eq. (4):

$$R_{oro}(x, y) = \iint \hat{R}(k, l) e^{i(kx+ly)} dk dl. \quad (6)$$

Note that ~~even~~ R_{oro} can attain negative values meaning a reduction of precipitation totals of superimposed processes. Even though $R_{oro} < 0$ might be mathematically possible, a negative total precipitation does not make sense physically and thus is
30 truncated away. Therefore, we set $R_{tot}(x, y) = \max(R_{oro}(x, y), 0)$.

The model has five internal free parameters that can be used to adjust/calibrate the model to the observations. Three of these parameters are implicitly considered in the transfer function (Eq. 4): the two time scales of τ_c and τ_f , which, however,

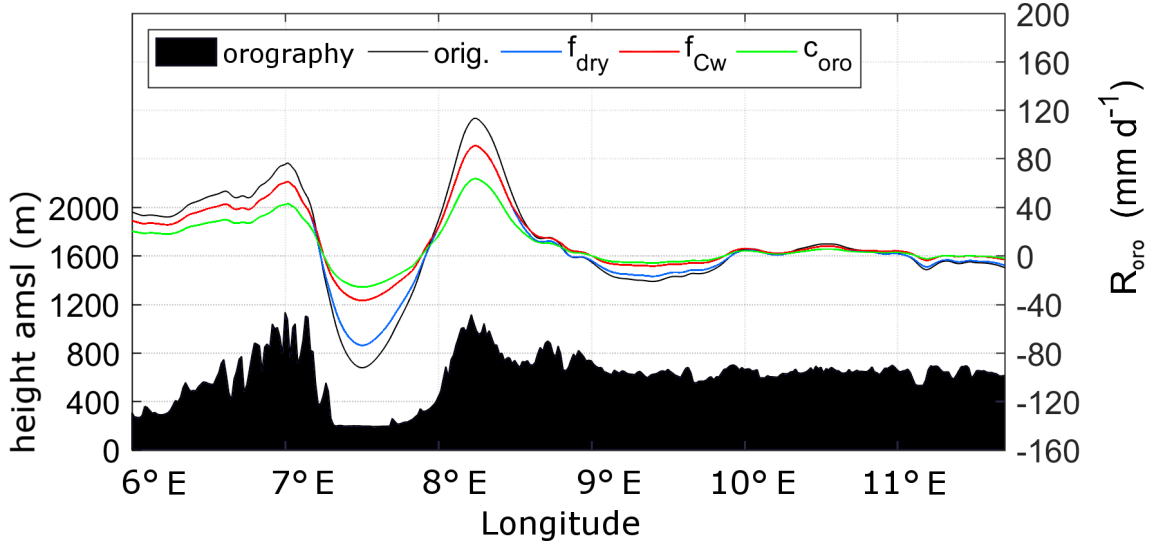


Figure 3. Different effects of the implemented internal free parameters f_{dry} (blue), f_{C_w} (red) and c_{oro} (green) on the original orographic precipitation part (black curve) for a west to east cross section through the model domain. The underlying orography is shown in black.

are virtually identical, and the uplift sensitivity factor C_w . The latter is modified with a multiplier to $C_w^* = f_{C_w} \cdot C_w$ with the new factor C_w^* replacing the original C_w in Eq. (4). f_{C_w} reduces the sensitivity of the model for lifting, and therefore, the precipitation rate is reduced, especially over mountainous terrain with sharp gradients, whereas in regions with less orographic gradients the effect is weak (Fig. 3, red curve). The used model formulation also allows for multiple ascents/descents of a virtual air parcel without any change in its water vapor content. Actually, water vapor is partly removed due to condensation processes during ascent, which is realized by f_{C_w} .

An additional parameter, f_{dry} , is implemented in Eq. (6) to reduce evaporation in descent regions, where $R_{oro} < 0$ is negative (Fig. 3, blue curve). The resulting underestimation of precipitation is found especially downstream of steeper mountains with greater descent (Kunz, 2011). ~~Therefore, we implemented a new (multiplicative) parameter~~ Parameter f_{dry} in (6), which is $f_{dry} < 1$ acts only at grid points (x, y) where $R_{oro} < 0$; and $f_{dry} = 1$, in which $f_{dry} < 1$; in all other cases $f_{dry} = 1$.

Finally, the last ~~and~~ additional calibration parameter, c_{oro} , reduces orographic precipitation in the whole domain (Fig. 3, green curve). It is a consequence of the assumption that the vertical lifting of an entire air column with saturation produces condensate and instantaneous fallout at any time, implying an overestimation of precipitable water. In reality, not all layers are completely saturated, and water may also partly be stored by clouds. Parameter c_{oro} is implemented similarly to f_{dry} in Eq. (6) but is independent of any lifting processes and constant for the whole areadomain. With these two parameters, orographic precipitation is modified to:

$$R_{oro}^*(x, y) = f_{dry} \cdot c_{oro} \cdot R_{oro}. \quad (7)$$

Note again that f_{dry} affects only grid points with net descent, whereas c_{oro} is constant over the whole domain. From a mathematical perspective the two factors f_{C_w} and c_{oro} could collapse to one single parameter. Nevertheless, they describe modifications on different physical processes as mentioned in the section above and, hence, have to remain separate.

2.3 Background precipitation

Background The background precipitation term R_{∞} (Eq. in (Eq. 1) describes the effect of large-scale lifting by synoptic-scale weather patterns. According to the ω -equation, lifting is the result of three different mechanisms: positive vorticity advection increasing with height (or vice versa); the maximum of diabatic phase transitions; and the maximum of warm air advection. Even though lifting is the superposition of these three mechanisms, it does not make sense to we do not split R_{∞} accordingly, as the single forcing terms can not be estimated out of radiosounding data. Furthermore, we assume that the large-scale conditions are almost horizontally homogeneous across the investigation area, and so is R_{∞} at each time step.

To simplify the inclusion of large-scale lifting in the SPM2D, we estimate R_{∞} from REGNIE totals observed rainfall totals (see Sect. 3.1) over a larger area with almost flat terrain, where R_{oro} as well as evaporation by ascent are minimized to a large degree are minimized. However, an analysis of various past events show shows the strong variability of the spatial distribution of precipitation even over flat terrain. For example, some events affect only the northern parts of the investigation area, whereas others only other occur only in the southern parts. To ensure the a proper estimation of R_{∞} , we choose an area that covers most of the total investigation area but excludes the Black Forest and prealpine lands. In the region, where we estimate R_{∞} (Fig. 4, black box), heavy rainfall is very unlikely. Totals of more than 50 mm per day, for example, exhibit an annual exceedance probability p of less than 0.5. Furthermore, as confirmed by Fig. 4, the probability of rain totals in excess of 50 mm per day is more or less homogeneously distributed. On average over 66 years, it can be assumed that precipitation in the area used for R_{∞} estimation mainly result results from large-scale lifting and to a lesser extent from orographic influences.

2.4 Frontal precipitation

Apart of from large-scale lifting connected to low-pressure systems or waves in the flow patterns, precipitation is also substantially enhanced by weather fronts. Active fronts may increase precipitation considerably due to cross-frontal circulations and lifting in the warm sector of a cyclone (e. g., Bergeron, 1937; Eliassen, 1962). Conversely, if a font front affects only parts of the investigation area (e.g., a trailing front, where the flow is almost parallel to the frontal alignment), regions outside the sphere of influence may experience much less or even no rain at all. Both effects are considered by implementing an additional quantity R_{front} in Eq. (1):

$$R_{\text{front}} = (R_{\text{oro}} + R_{\infty}) \cdot (c_{\text{front}} - 1), \quad (8)$$

where c_{front} serves as the enhancement or reduction factor of the overall precipitation. In this simple parameterization, R_{oro} is considered again because frontal precipitation is additionally enhanced by orography as shown, for example, by Browning et al. (1975) or Houze and Hobbs (1982). Due to the additive superposition of all precipitation components in Eq. (1), we have to subtract the original precipitation totals leading to a total multiplier $(c_{\text{front}} - 1)$. The frontal enhancement factor is a function

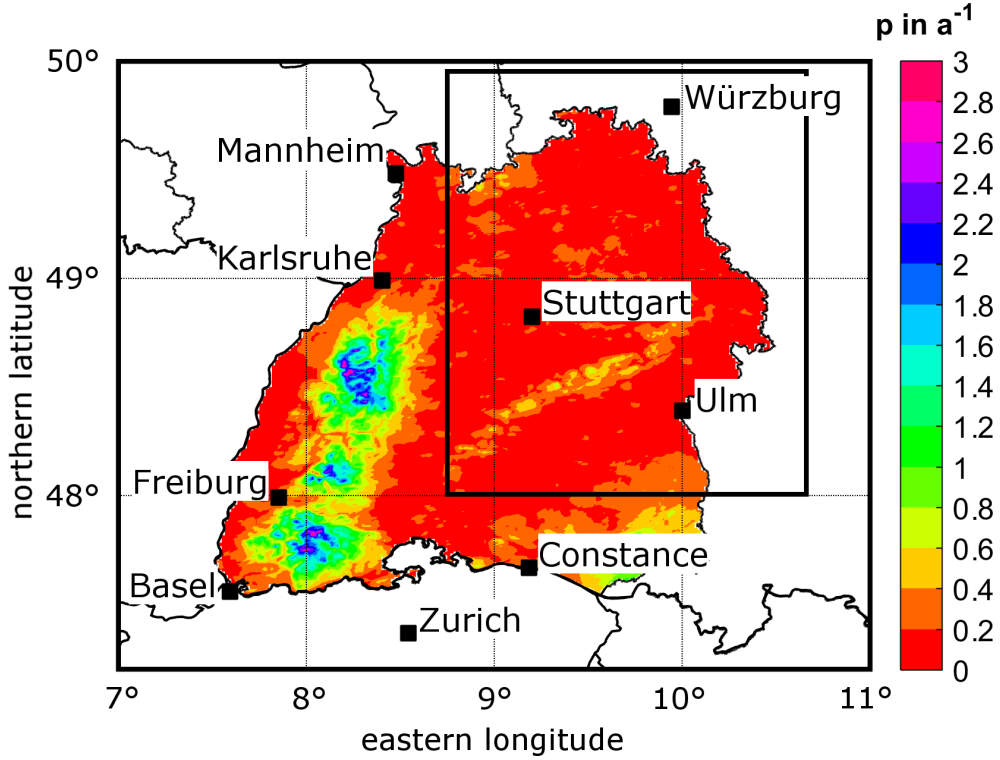


Figure 4. Probability of observed 24-hour REGNIE-rainfall totals greater than 50 mm expressed as the average days per year for Baden-Württemberg; the black box indicates the area, where background precipitation R_∞ is estimated.

of space realized by a rectangular area $c_{\text{front}}(x, y)$ (Fig. 5), where the orientation of the y -axis is prescribed by the mean wind direction β (Fig. 5).

- 5 To avoid strong gradients at the border areas of the rectangular, we applied Gaussian-shaped smoothing. Along the x -dimension, the spread is set to $8\sigma_n$, where σ_n is the standard derivation of the normal distribution. In the y -direction, an infinitesimal length is considered (Fig. 5). As the minimum of c_{front} is zero, R_{front} can also attain negative values, thus leading to a weakening of total precipitation in an area affected or not affected by a front. ~~To~~ In order to calculate c_{front} from the observational data, we define this quantity as the relative difference between observations O (REGNIE) and output M of the
- 10 rSPM (neglecting embedded convection as described in the next paragraph). This is expressed by

$$c_{\text{front}} = \bar{O} \cdot \bar{M}^{-1} \quad (9)$$

assuming that the differences originate primarily from frontal effects. For the quantification of c_{front} , we use spatial mean values over the investigation area \bar{O} and \bar{M} . ~~The corresponding pdf for stochastic modeling is estimated using the least QRS method with seasonal differentiation.~~ for a training sample of historic heavy precipitation events (see Sect. 2.6).

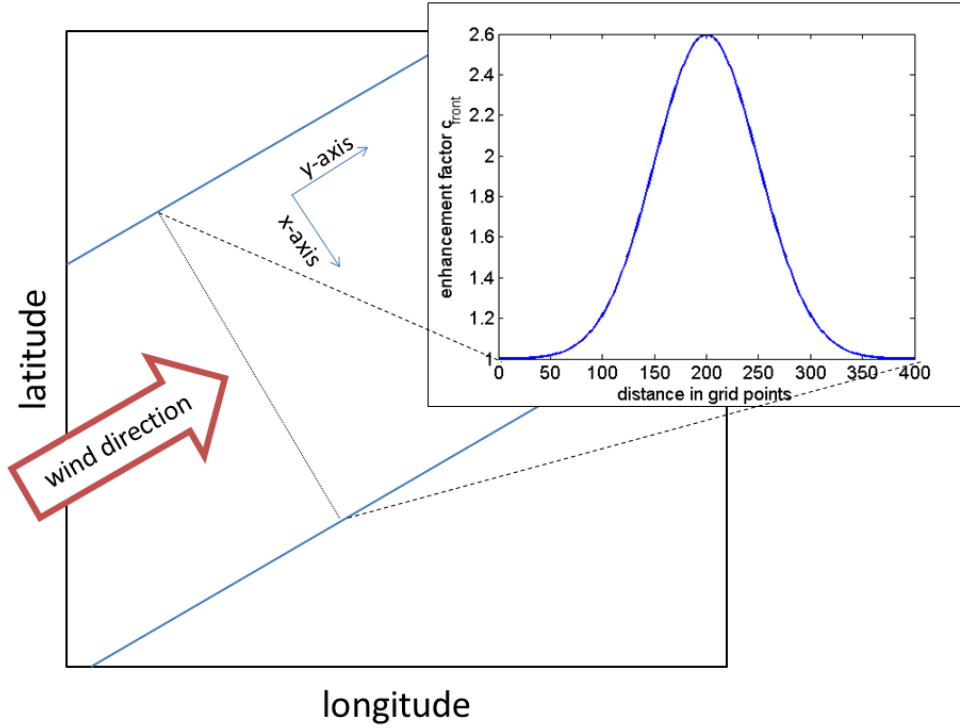


Figure 5. Schematic of a Gaussian-shaped distribution of the frontal enhancement factor with $c_{\text{front}} = 2.6$ and $\sigma_n = 50$ (upper right corner) and its location in the model domain for a southwesterly wind direction (arrow). The blue lines indicate the boundaries of the frontal zone.

2.5 Embedded Convection

The last part of the total precipitation model SPM2D considers convection embedded in mainly stratiform clouds (e. g., Fuhrer and Schär, 2005). Note, however, that the model is not foreseen to simulate purely convection. Such embedded convection mainly occurs when lifting is locally enhanced at mid- and upper tropospheric levels leading to a decrease of thermal stability by the release of the latent heat of condensation (e. g., Kirshbaum and Durran, 2004; Kirshbaum and Smith, 2008; Cannon et al., 2012). Convection in general involves several complex processes that make simulation a difficult task. Since our model is restricted to large-scale precipitation with the objective of quantifying extremes in terms of areal precipitation solely, we treat embedded convection in a very simplified way by implementing several rectangular cells similar to the approach of frontal system consideration.

Because embedded convection is also partly induced by orographic precipitation mechanisms, we implemented a multiplicative factor to the precipitation fields related to both orographic and large-scale lifting, similar to the frontal part:

$$R_{\text{conv}} = c_{\text{conv}} \cdot (R_{\text{oro}} + R_{\infty}), \quad (10)$$

with enhancement factor c_{conv} .

For each time step of the simulation, we choose a number of convective cells, each with specific width W and length L , and distribute ~~these~~~~them~~ randomly over the whole model domain (Fig. 6). Both width W and length L of each rectangle of the convective cells are estimated from the characteristics of the severe convective storms identified from radar data by ~~Fluck, 2018~~ (see Sect. 3.3). Furthermore, we restricted the two parameters to $L > W$ and $L_{\max} = 300$ km, or 300 grid points, respectively. As for the frontal systems, the wind direction defines the orientation of the longer sides of the rectangles. For each convective cell, we choose $L \cdot W$ specific factors c_{conv} with $c_{\text{conv}} \in \{0; 1\}$. As found, for example, by Fuhrer and Schär (2005) or Cannon et al. (2012), embedded convection can enhance precipitation up to 200%; thus, the given range of c_{conv} is adequate. Within the single cells, the spatial distribution of c_{conv} randomly varies between the given ~~borders~~~~limits~~. Summing up all cells enables ~~the existence of~~ more than one cell per day at a specific grid point. The complete convective precipitation field for each time step is spatially smoothed to avoid sharp gradients. ~~Opposite of~~~~In contrast to~~ the Gaussian shape smoothing due to a more or less continuous ~~ascent~~~~increase~~/~~descent~~~~decrease~~ of precipitation enhancement in the case of fronts, we use a moving average with a span of 10 grid points to preserve the high spatial variability of convection.

2.6 Event definition and statistical distribution functions

Stochastic modeling of precipitation events with SPM2D requires the adjustment of appropriate probability density functions (pdfs) to all input parameters. These pdfs are estimated from an adequate set of past heavy rainfall events. Based on the pdfs, several thousands events can be stochastically generated. Because the characteristics of the ambient conditions and thus the precipitation regimes change throughout the year, we seasonally differentiate the estimated pdfs among spring (MAM), summer (JJA), autumn (SON), and winter (DJF).

In the first step, a sufficient and appropriate subset of relevant historic events has been identified. An event here is defined as a period of one or more days with persisting precipitation above a certain threshold of daily precipitation. Because our study focuses on major large-scale flood events and not on local-scale floods or flash floods, an extension to multi-day events is reasonable to consider time delays in discharge response or flood waves traveling along river networks (e. g., Duckstein et al., 1993; Uhlemann et al., 2010; Schröter et al., 2015).

We define the historic event set based on maximum areal precipitation. For this, we simply accumulate the (equidistant) 24-hour rainfall totals \bar{R}_{BW} of all grid points in BW (see Sect. 3.1). Following the sorting of all values of \bar{R}_{BW} in descending order, the strongest 200 values enter the sample (top200). As precipitation is not limited to these (single) days but may be embedded in longer time periods, we define the threshold R_{thres} for event definition. Estimating R_{thres} , we consider “wet” days by using $\bar{R}_{\text{BW}} > 0$ solely, and set R_{thres} to the 75% percentile of this sub-sample. A lower threshold leads to an over-interpretation of longer clusters, a higher one avoids multi-day events.

Event precipitation starts on the first day that exceeds R_{thres} . When areal means of consecutive days are also above R_{thres} , they are simply accumulated, yielding events of more than one day. The last day with $R > R_{\text{thres}}$ before a period of at least three days of non-exceedance defines the end of an event. Such a three-day period ensures statistical independence of the events in accordance with the approach of Palutikov et al. (1999) for wind storms. Following Piper et al. (2016), we only count “rain days” ($\bar{R}_{\text{BW}} > R_{\text{thres}}$) and neglect “skip days” ($\bar{R}_{\text{BW}} < R_{\text{thres}}$) in between the start-day/end-day period for

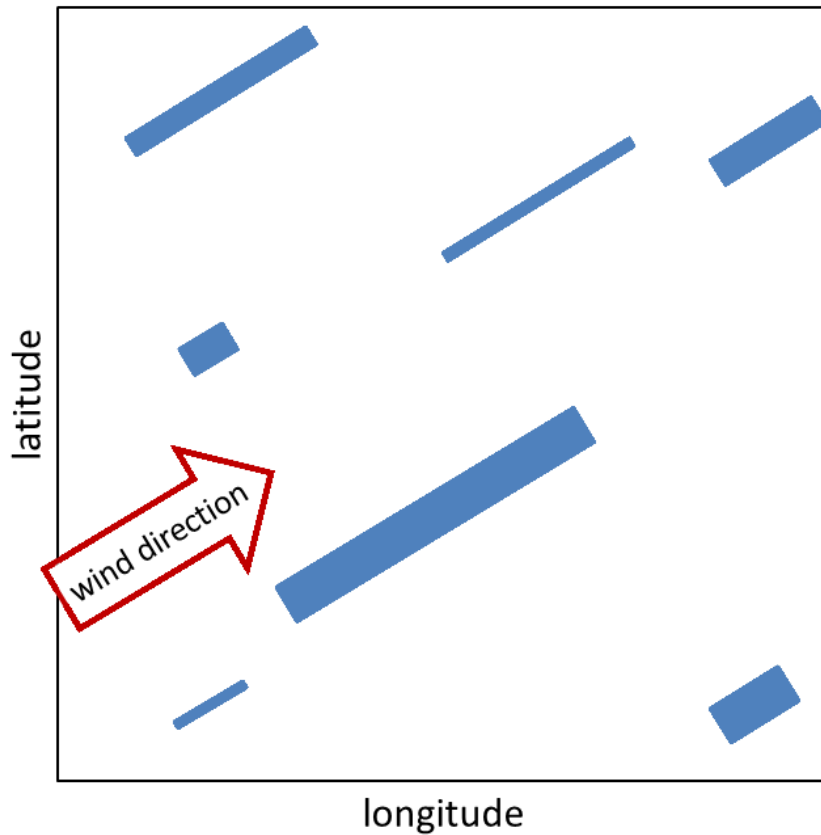


Figure 6. Schematic of the convection implementation with rectangular cells (blue). The orientation is defined by the wind direction (arrow); each cell is assigned to an individual factor c_{conv} .

event duration estimation, which is a widely used approach (Wanner et al., 1997; Petrow et al., 2009). This approach avoids the over-interpretation of longer clusters.

5 Based on the procedure described above, a defined precipitation event contains one or more days of the top200 sample. For this event set, all required input parameters were extracted from sounding data and rainfall totals (see Sect. 3).

In the next step, we identified the pdfs most appropriate for statistically describing each of the seven atmospheric input parameters, event duration t_{ex} , background precipitation R_{∞} and front factor c_{front} . In addition to 20 pdfs preset by the MATLAB statistic toolbox (MATLAB, 2016), we considered the circular von-Mises distribution (Mardia and Zemroch, 1975)
 10 for wind direction only. In total, 17 pdfs were suitable, and tested and compared with the distribution of each parameter for each of the four seasons (Table 1). Note that Gumbel (GbD) and Weibull (WbD) distributions are special cases of the generalized extreme value distribution (GEV) and that some pdfs cannot be used for every parameter due to their ranges of validity.

To find the pdf that best fits the data, we estimated the appropriate number of histogram classes according to Freedman and Diaconis (1981), and we calculated the bias, root mean square error (rmse) and Spearman correlation coefficient r_{sp} (Spearman, 1904) as quality indicators (QIs). We also applied a χ^2 -test according to Wilks (2006) as a QI. For each QI, we ranked the pdfs in ascending order and added up the rank numbers for each pdf receiving the best fit in terms of the least QI-rank sum (QIRS). In the case of alikeness of two or more pdfs (about 10 % of all cases), we manually selected the best one.

3 Data sets

The SPM2D presented in this study is based on two different types of data sets: gridded precipitation data to estimate background precipitation and to calibrate and verify the model, and vertical profiles from radiosondes to initialize the model. Furthermore, the SPM2D is also validated with reanalysis data done with the regional climate model of the Consortium for Small Scale Modeling (COSMO-CLM). Unless otherwise indicated, the investigation period covers the years of 1951–2016 (hereinafter referred to as IP).

3.1 Rainfall totals

Rainfall statistics in our study are based on the REGNIE (German: *REGionalisierte NIEderschläge*; regionalized precipitation) data set provided by the German Weather Service (Deutscher Wetterdienst; DWD). REGNIE is a gridded data set of 24-hour totals based on several thousand climate stations more or less evenly distributed across Germany (so-called RR collective). The REGNIE algorithm interpolates the observations to a regular grid of approximately 1 km² considering elevation, exposition, and climatology (Rauthe et al., 2013). The REGNIE domain covers the area with $5.83^\circ \text{ E} < \phi < 16^\circ \text{ E}$ and $47^\circ \text{ N} < \theta < 55.08^\circ \text{ N}$

Table 1. List of the tested and suitable pdfs preset in the MATLAB statistical toolbox (the short acronyms in brackets are for further orientation).

<u>Birnbaum-Saunders (BSD)</u>	<u>Nakagami (NkD)</u>
<u>Gamma (GmD)</u>	<u>Normal (ND)</u>
<u>Generalized Extreme Value (GEV)</u>	<u>Poisson (PD)</u>
<u>Gumbel (GbD)</u>	<u>Rayleigh (RyD)</u>
<u>Half-Normal (HND)</u>	<u>Rician (RcD)</u>
<u>Inverse Gaussian (IGD)</u>	<u>Stable (SD)</u>
<u>Logistic (LD)</u>	<u>Student's t (StD)</u>
<u>Log-Logistic (LLD)</u>	<u>Weibull (WbD)</u>
<u>Log-Normal (LND)</u>	

(ϕ : longitude; θ : latitude). Grid points outside of Germany are set to a missing value. The observation period is from 06 to 06 UTC.

5 It should be noted that REGNIE data are temporally not homogeneous due to changes in the locations and number of rain gauges. Furthermore, areal precipitation exhibits a certain bias especially over elevated terrain, such as the Black Forest mountains, because the number of stations considered by the regionalization is limited. Its magnitude, however, cannot be directly estimated from the observations (Kunz, 2011).

10 We use the REGNIE data set for the definition of the top200 data set, event duration, background precipitation and the front factor c_{front} , and for the validation of the SPM2D.

3.2 Radiosoundings

15 Input of the SPM2D are seven atmospheric parameters derived from radiosoundings: thermal stability in terms of saturated Brunt-Väisälä frequency N_m (e. g., Lalas and Einaudi, 1973) and actual and saturated vertical temperature gradients (γ and Γ_m), water vapor scaling height H_w , water vapor mixing ratio q_v , wind speed U , and direction β (see Sect. 2). These parameters are computed from the vertical profiles of temperature, moisture, wind speed, and direction at the radiosounding station of Stuttgart (48.83° N 9.20° E) located somewhat downstream of the northern Black Forest mountains. Even though the location might not be ideal because the profiles do not represent undisturbed conditions, the profiles are similar to that of the upstream station of Nancy in France as shown by Kunz (2011) for heavy rainfall events on average. Data from Nancy, however, are available after 1990 only and, thus, cannot be used in this study, whereas soundings from Stuttgart are available since 1957.

20 We used the soundings at the main standard times for synoptic observations (00 and 12 UTC).

Sounding data were provided by the Integrated Global Radiosonde Archive (IGRA) for quality-controlled radiosonde and pilot balloon observations from the National Climatic Data Center (Durre et al., 2006). These data, available at both main pressure levels and levels of significant changes of one of the parameters, were interpolated into equidistant increments of $\Delta z = 10$ m (Mohr and Kunz, 2013). All parameters derived from the soundings refer to the lowest 5 km of the atmosphere since this layer is most relevant for air flow and stability. Furthermore, to account for the decreasing impact of higher atmospheric layers on the flow characteristics, all flow parameters Λ have been vertically integrated ($\tilde{\Lambda}$), with a water vapor weighting being applied (Kunz, 2011):

$$\tilde{\Lambda} = \frac{\int_{z=0}^{z_t} \Lambda \rho_d q_v dz}{\int_{z=0}^{z_t} \rho_d q_v dz}, \quad (11)$$

where ρ_d is the density of dry air and $z_t = 5000$ m.

30 As some layers may be moist-unstable, resulting in imaginary N_m , the averaging routine is applied to N_m^2 . In the few cases where \tilde{N}_m was imaginary, it was set to a near-neutral, constant value of 0.0003 s^{-1} .

3.3 Parameters for Embedded Convection

Embedded convection in the SPM2D is considered by single streaks of enhanced precipitation (see Sect. 2.5). These streaks are stochastically generated according to the statistical distributions of the observed maximum length L and width W of severe convective storms estimated by Fluck (2018). In that study, convective storms were identified from the constant altitude plan position indicator (CAPPI) for a reflectivity in excess of 55 dBZ, also known as the Mason (1971) criterion for hail detection. The application of a tracking algorithm based on the concept of the algorithm of TRACE3D (Handwerker, 2002) yields entire tracks of convective storms. In total, more than 20,000 tracks over Germany, France, Belgium, and Luxembourg were identified during the summer half years (April to September) in the period 2004–2014. Even though we do not consider rainfall related to severe convective storms or hail in the SPM2D, the statistical distributions of the storm’s dimensions are reliable proxies for the extension of enhanced precipitation from embedded convection described by R_{conv} .

3.4 Numerical Weather Simulations

Simulation results from the SPM2D are validated with rain totals from the non-hydrostatic Consortium for Small-scale Modeling (COSMO) model in climate mode (CCLM Rockel et al., 2008). CCLM is run by global ERA-40 reanalysis from the European Center for Medium-Range Weather Forecasts (ECMWF) with a resolution of T159, which corresponds to approximately 125 km on 60 vertical layers (Källberg et al., 2004). The ERA-40 is available for the period from September 1957 to August 2002 and includes the assimilation of several observational data sets such as satellite data. Laube (2018) performed a dynamical downscaling of ERA-40 to a horizontal resolution of 2.8 km for Southern Germany using a threefold regional nesting (50, 7, to 2.8 km). High-resolution CCLM data is available for the period 1971–2000. For the evaluation, we considered the top200 REGNIE events, from which around 100 events occurred within the period where CCLM data are available including the top two and 7 (14) of the strongest 10 (20) events.

4 Calibration

This section describes the calibration of the SPM2D by comparing modeled and observed precipitation fields (REGNIE 24-hour totals). The outcome is a combination of the free parameters with the highest skill of the simulated rainfall totals-historic rainfall totals (training sample), which then is used for the stochastic simulations of 10,000 rainfall events, which (validation sample). The latter is equivalent to a period of several thousand years as described in Sect. 6. At the end of this section a concise study on model sensitivities is given.

4.1 Method

Based on the event set of top200, the free model (calibration) parameters, τ^* , f_{C_w} , f_{dry} and c_{oro} , are assessed based on the event set of top200. All other parameters required by the SPM2D (cf. Sect. 2) are quantified from radiosounding profiles at Stuttgart. In this evaluation, the stochastic components of the SPM2D and the randomly modeled components for fronts (R_{front}) and embedded convection (R_{conv}) are neglected. Without these components, the model is referred to as the reduced SPM2D (rSPM).

~~To~~In order to determine appropriate values of the free parameters, a large number of model simulations was carried out with the rSPM. Whereas one parameter was successively varied, the others were kept constant. The selected ranges and increments of the parameters listed in Table 2 resulted in 2,016 possible parameter combinations, giving a total number of approximately 390,000 simulation days for the top200 event set. For each day and parameter combination, we assess the model skill by quantifying both bias and rmse. Both data sets (model output and REGNIE) are slightly smoothed using a running 5×5 grid box. The reason for the smoothing is that REGNIE data, despite having a high resolution of 1 km, exhibit spatial uncertainty due to the limited number of observational data considered. Especially around the crests of Black Forest, where the number of stations is very low, REGNIE data cannot reproduce local peak rainfall totals. Furthermore, as shown, for example, by Barstad and Smith (2005), smoothed data yield more robust results when comparing model and observation data. Note, however, that larger values ~~for~~of τ^* and smaller values of f_{C_w} , respectively, likewise smooth the simulated precipitation fields. In these cases, the QIRS method used for the evaluation (Sect. 2.6) has to be applied carefully.

To avoid apparently better representations of smoothed data fields, we use skill score S (Eq. 12) described by Taylor (2001) for evaluating climate models to determine the best parameter combination of rSPM:

$$S = \frac{4(1+r)}{\left(\hat{\sigma}_f + \frac{1}{\hat{\sigma}_f}\right)^2 \cdot (1+r_0)}, \quad (12)$$

where r is the correlation coefficient after Spearman (1904), r_0 the maximum attainable correlation, and $\hat{\sigma}_f = \sigma_{\text{mod}} \cdot \sigma_{\text{obs}}^{-1}$ the normalized standard deviation with the standard ~~deviation~~deviations of model output σ_{mod} and ~~that of~~ observations σ_{obs} . For $\hat{\sigma}_f \rightarrow 1$ and for $r \rightarrow r_0$, S approaches unity, which is the best result. According to Taylor (2001), improved values of rmse or bias ~~does not mean~~do not lead to an actual improvement of the model performance, and the use of correlation and standard deviation is more stable. Furthermore, Taylor (2001) provided no regulation for the estimation of r_0 . Therefore, we set r_0 to the maximum calculated correlation coefficient of all simulations. As it is not guaranteed that this maximum is the actual maximum attainable correlation, we increase r_0 by 10%, ~~which yields~~ %, yielding $r_0 = 0.93$.

Skill score S is computed for each simulation day and each parameter combination. From all realizations, we select the parameter combination that yields the highest median value of S averaged over all top200 events, as the SPM2D should be able to properly represent a broad range of different atmospheric conditions.

Table 2. The minimum and maximum values, and the increments of the time scales τ^* , and multiplicative factors for the uplift sensitivity f_{C_w} , the lee-side drying f_{dry} , and the adjustment of orographic precipitation c_{oro} .

parameter	minimum	maximum	increment
τ^*	800 s	1500 s	100 s
f_{C_w}	0.5	1.0	0.1
f_{dry}	0.4	1.0	0.1
c_{oro}	0.5	1.0	0.1

4.2 Calibration Results

Applying the method to the top200 events as described above, the highest median skill score of $S = 0.60$ is obtained for the combination of $\tau^* = 1400$ s, $f_{C_w} = 1.0$, $f_{dry} = 0.4$ and $c_{oro} = 0.8$. For this combination, the other median values of the other quality indices are $r_{SP} = 0.39$, $\hat{\sigma}_f = 0.98$, bias = 6.30 mm, and rmse = 14.85 mm. The assessed values for the former two model parameters are physically plausible and comparable to other studies with the rSPM (e.g., Barstad and Smith, 2005; Caroletti and Barstad, 2010; Kunz, 2011). The latter two parameters are incorporated exclusively in this study. However, considering the slight overestimation of orographic precipitation enhancement and the strong overestimation of lee-side drying, the two values are also physically plausible seem to be physically plausible as well.

The sensitivity of skill score S to τ and of to the two other parameters, f_{C_w} and c_{oro} (Fig. 7), shows a dipole structure in both cases with the highest values of S along a counter diagonal. Minor skill scores obtain are obtained with the shortest (longest) time scales in combination with the highest (lowest) uplift sensitivity or highest (lowest) weighting of R_{oro} in Eq. 1 (Eq. 1). This implies, on the one hand, that for smaller displacements of precipitation from the formation region, orographic precipitation is overestimated by the rSPM and thus has to be reduced. On the other hand, R_{oro} has to increase for wider displacements.

Note, however, that the above-identified parameter combination yields the lowest errors only when averaging over all events. Single events may become more realistic with another parameter combination, reflecting particularly the unknown, and thus not considered microphysical processes that are decisive for precipitation formation and that are strongly controlled by vertical wind speed, temperature, and moisture profiles. The dependency of microphysical processes on ambient conditions, however, is not relevant when running the model in the stochastic mode as in this study.

4.3 Sensitivity of simulated total precipitation

To demonstrate how atmospheric conditions translate into precipitation, we conduct a sensitivity study with rSPM using the top200 event set by gradually changing the input parameters. Following Kunz (2011), we perturbed the values of N_m^2 , q_v , U , β , and τ estimated from the top200 events. This is done by multiplying the respective quantity with var mult increasing linearly from 0.5 to 2.0 in increments of 0.1. Wind direction β is varied in the range of $\pm 30^\circ$ in increments of 5° . The calibration parameters are set to their optimum values estimated in the previous section. Besides areal mean precipitation, we analyze rmse and skill score S for the median over the top200 event set.

Areal mean precipitation accumulated over 24 hours shows a high sensitivity to changes in water vapor content q_v , wind speed U and wind direction β (Fig. 8). In all cases, precipitation increases (decreases) with increasing (decreasing) parameter values. Lowest sensitivity occurs for β between $\pm 15^\circ$ because of the orientation of the major orographic structures (e.g., the Black Forest) from southwest to northeast. Westerly inflows, prevailing on average, still occur for small variations of β . For greater shifts ($\Delta\beta > 20^\circ$ or $\Delta\beta < -20^\circ$), when the inflow angle becomes smaller, sensitivity slightly increases. The changes in the wave regimes and, thus, the location of the updraft may also explain the partly stepwise form of the curves for both β and U . The results for varying stability N_m^2 and microphysical time scales τ reveal an opposite behavior of areal mean with an

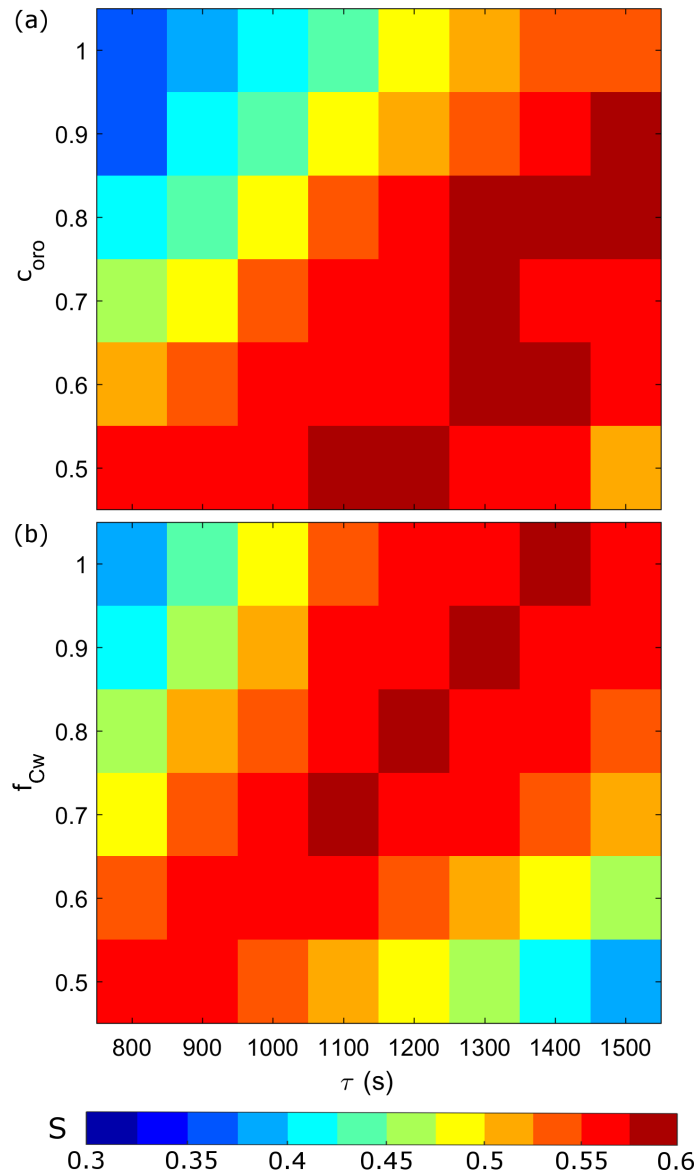


Figure 7. Sill score S , averaged over the top200 event set, depending on τ and (a) c_{oro} , and (b) f_{Cw} , while the other free parameters, respectively, were set to their optimum values.

increase at smaller values and vice versa. Furthermore, the sensitivity of the model to changes of these two parameters is much weaker compared to the other parameters.

Qualitatively a similar behavior of the model is found for the medians of rmse and skill score S (Fig. 9). While areal precipitation discussed above only provides insights how changes in the ambient parameters feedback into rainfall, rmse and

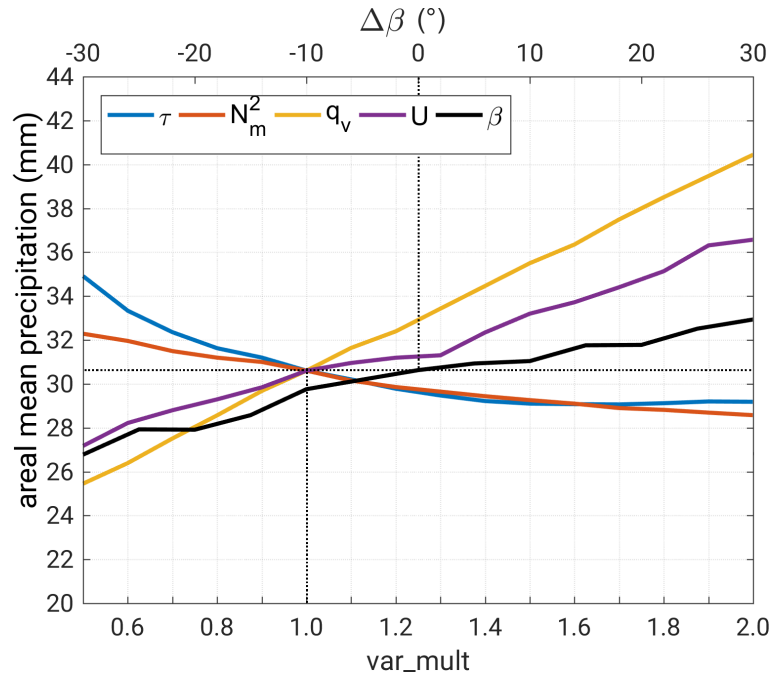


Figure 8. Areal mean precipitation (median of the top200 BW event set) as a function of N_m^2 , q_v , U , β , and τ perturbed by a multiplicative factor ($0.5 \leq var_mult \leq 2$) and changed $\Delta\beta$. The dotted lines indicate the values of the reference run.

S also consider its spatial distribution. The results for rmse (Fig. 9a) again reveal the highest sensitivity of the rSPM to changes in q_v and U . While for $var_mult > 1$ the sensitivity in terms of rmse is similar to areal precipitation, there is a much higher sensitivity for values below 1. In those cases, orographic precipitation is more detached to the mountain crests resulting in higher totals due to reduced evaporation in the descent regions. Because of the combination of higher totals at different locations, rmse show a higher sensitivity to changes of τ and N_m^2 compared to areal mean precipitation.

The skill score S , on the other hand, is most sensitive to changes in q_v and τ (Fig. 9b). Regarding N_m^2 , S decreases just for very high values of var_mult , while there is almost no sensitivity on the wind direction β . In all cases, highest S is obtained for the original values of the input parameters ($var_mult = 1$ or $\Delta\beta = 0^\circ$), indicating the well calibration of the model.

10 4.4 Case Study

After the parameter adjustment, the rSPM tends to slightly underestimate orographic precipitation, whereas totals over flat or rolling terrain are overestimated. This behavior can also be seen, for instance, in the example of 31 May 2013 (Fig. 10), a heavy precipitation event that triggered the severe flooding in 2013 (Schröter et al., 2015).

On that day, a pronounced low pressure system with its center over Croatia led to the sustained advection of moist airmasses from northerly directions around 20° in combination with synoptic-scale ascent. The Stuttgart sounding with low stability

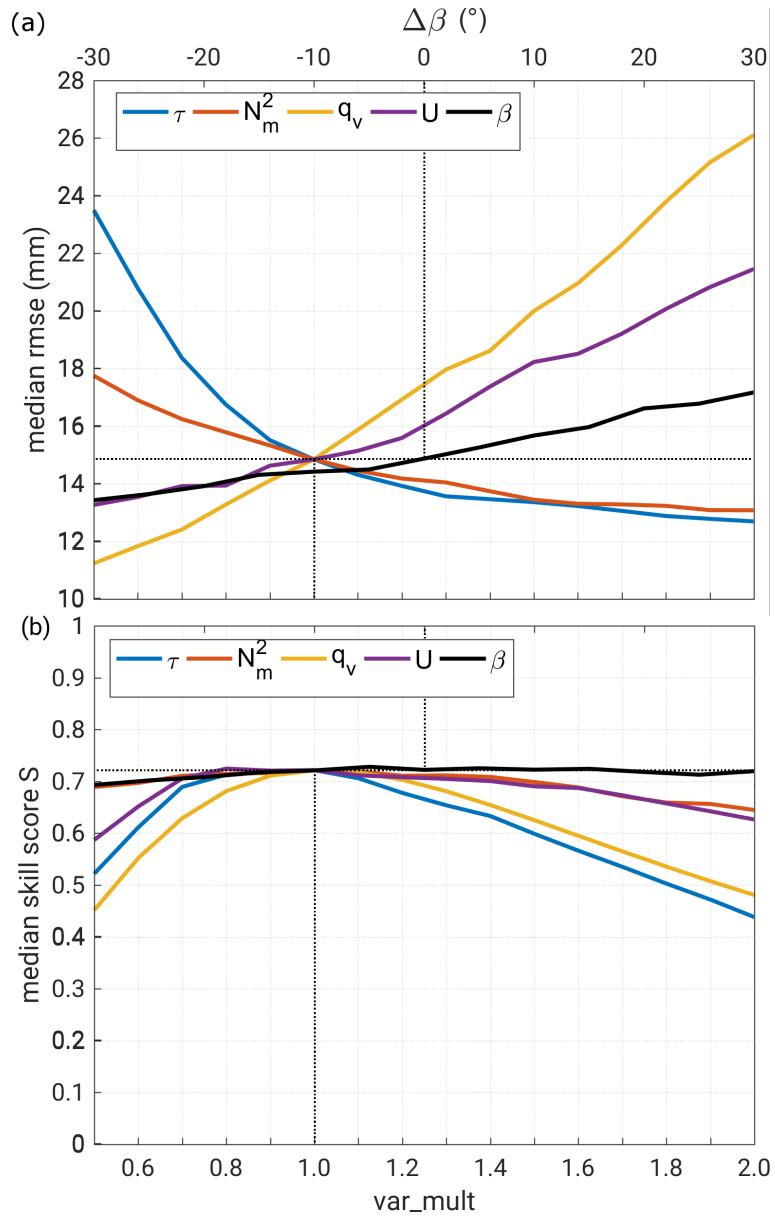


Figure 9. Same as Fig. 8, but for (a) median rmse and (b) median skill score S .

($N_m = 0.0055 \text{ s}^{-1}$), high precipitable water ($pw = 24 \text{ kg m}^{-2}$), and high wind speed ($U = 20 \text{ m s}^{-1}$), the latter two determining the horizontal water vapor flux, is already an indication of high precipitation totals, especially over the Northern Black Forest. Consequently, precipitation totals across the investigation area were reached values between 10 and 100 mm.

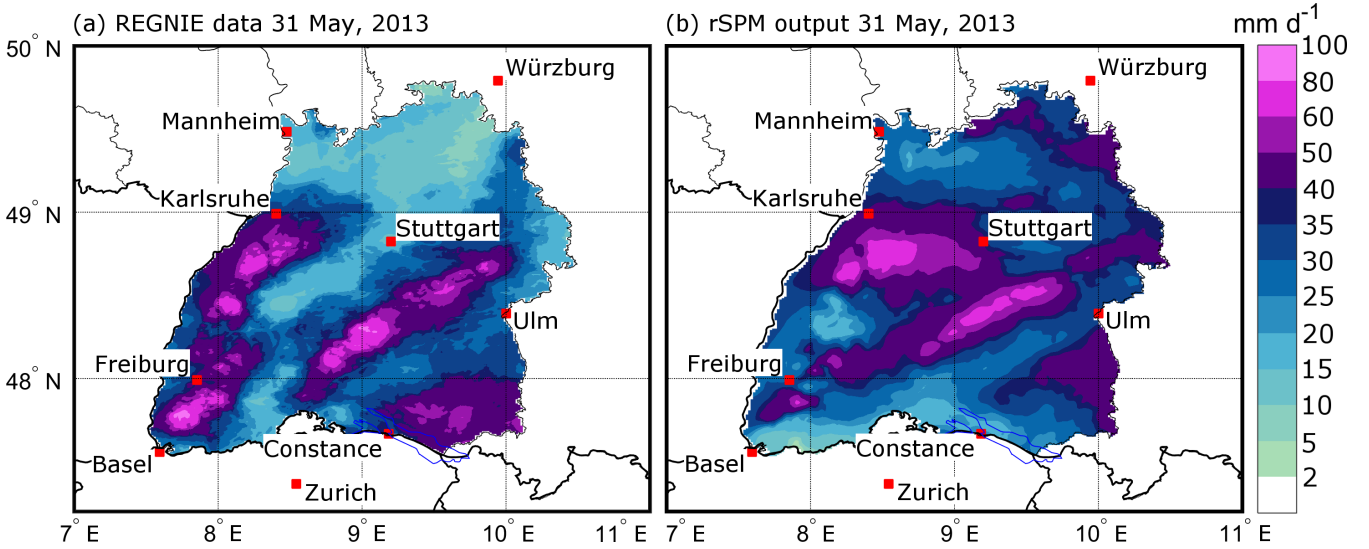


Figure 10. Comparison of (a) REGNIE 24-hour rainfall totals, and (b) rSPM output for Southwest Germany, exemplary on 31 May, 2013. Note that REGNIE data are available for Germany only. The parametrization in (b) is $\tau^* = 1400$ s, $f_{C_w} = 1.0$, $f_{dry} = 0.4$, and $c_{oro} = 0.8$. The areas outside of Baden-Württemberg are covered white for better visualization and comparison.

Overall, the rSPM is able to reproduce most of the structures of the observed rain field (Fig. 10). The quality indices for that day are $S = 0.62$, $r_{Sp} = 0.30$, $\hat{\sigma}_f = 0.75$, bias = 4.44 mm, and rmse = 14.82 mm. The best agreement between observed and simulated precipitation fields is found for the Northern Black Forest as well as Swabian Jura. Over the northern part of the model domain (north of 49° N) and southwest of Stuttgart, simulated rainfall is substantially higher compared with REGNIE. By contrast, the rSPM simulates lower totals in the Southern Rhine Valley near and over the mountainous regions of the Southern Black Forest (around Freiburg), especially east of the Basel region, where lee-side evaporation in the model dominates.

One reason for the discrepancy between observed and simulated precipitation might be the ~~improper ill-suited~~ location of the Stuttgart sounding used for the model initialization. ~~Since orographic precipitation in the rSPM strongly depends on the initial conditions of the used sounding data, which may be affected by the upstream terrain of northeastern Baden-Württemberg, we conduct a sensitivity study of this event by varying the ambient conditions. Following Kunz (2011), we perturbed the estimated values for N_m^2 , q_v , U , and τ by multiplicative factor var_mult increasing linearly from 0.5 to 2.0 in increments of 0.1. Wind direction β was varied in the range of $\pm 30^\circ$ in increments of 5° .~~

~~The~~ The sensitivity study as described in Sect. 4.3 for this particular event obtains the best results in terms of the lowest rmse (Fig. 11) ~~are obtained~~ for higher stability (increase of N_m^2) or longer time scales, whereas in the case of water vapor density q_v or horizontal wind speed U , the lowest rmse is obtained when decreasing the original values. The results also reveal a higher sensitivity of the rSPM to changes in water vapor and wind speed ~~compared with stability or microphysical time scales~~ for

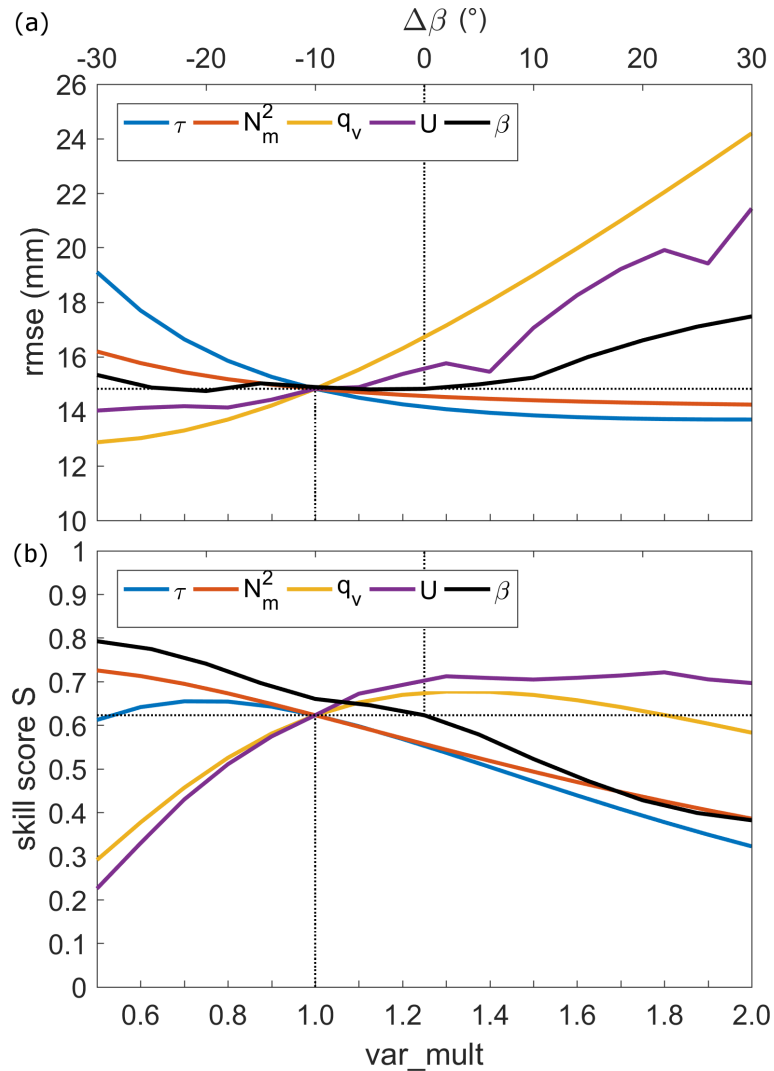


Figure 11. Changes of (a) rmse, and (b) skill score S for perturbed values of N_m^2 , q_v , U , β , and τ , with a multiplicative factor (var_mult), and changed $\Delta\beta$, for 31 May, 2013. The dotted lines indicate the values of the reference run.

[this event](#). Regarding wind direction β , ~~only small changes can be detected for $\Delta\beta$ between -30° and $+10^\circ$ with the lowest rmse is given~~ for the original value. ~~The main reason for this is the orientation of the major orographic structures (e.g., the Black Forest) from southwest to northeast, for which variations of β become relevant only for more easterly shifts ($\Delta\beta > 10$), resulting in a steeper inflow angle.~~

The highest skill score S , conversely, is reached for increasing U and q_v , and decreasing τ and N_m^2 . In the case of wind direction, S continuously decreases from 0.8 in the northwesterly inflow to 0.4 in the northeasterly winds.

For the case study of 31 May 2013, the observed mean for Baden-Württemberg is $\bar{R}_{\text{obs}} = 33.1$ mm, whereas the simulated mean is $\bar{R}_{\text{mod}} = 37.3$ mm, and thus, only 12.6 % higher compared with the observations. The rmse and skill score S are near the optimum when perturbing different variables. The deviations of spatial means and quality indices are at a reasonable level.

5 However, as already explained, the SPM2D is not designed to represent historic events in detail. Other parameter combinations of f_{C_w} , f_{dry} , C_{oro} and τ^* may yield even better results for this single event.

5 Parameter estimation for the stochastic simulations

5.1 Adjustment of the distribution functions

Stochastic model simulations are based on pdfs that are adjusted to the required parameter. Event duration τ , as well as back-
10 ground and frontal precipitation as well as preconditions are estimated from REGNIE data for the top200 event set. Ambient parameters required by the SPM2D are derived from vertical profiles of the radiosondes at Stuttgart, whereas the width extent of embedded convection is estimated from the radar tracks of severe convection. Furthermore, as mean ambient conditions and thus precipitation characteristics change throughout the year, we differentiate among the four seasons.

After separating the historic event set into the four main seasons, we estimate for each of the 10 parameters the pdf that best
15 fits the distribution of the observations (= 10 parameters \times 4 seasons = 40 cases; Table 3) by using the least QIRS method (cf. Sect. 2.6). From the overall 21 pdfs that were considered, only 12 are suitable for adjusting the observations. In most of the cases, the GEV with its special realizations of Gumbel (GbD) and Weibull (WbD) distribution appears to be appropriate (26 distributions), followed by the inverse Gaussian pdf (IGD) for five parameters and the Gamma pdf (GmD) for three parameters. Especially for flow parameters derived from the soundings, GEV appears to be the most appropriate (19 out of 28 cases). In
20 five out of 40 cases (≈ 12.5 %), we had to choose the pdf manually due to the likeness of two pdfs according to the QIRS method.

The input parameters are considered as independent and uncorrelated. To justify this assumption, we perform a correlation analysis of all possible combinations of input parameters using the correlation coefficient of Spearman (1904). In total, a low number of about 16 % have a correlation coefficient above ± 0.5 and only 4 % are highly correlated with ± 0.7 . Regarding
25 these cases, 90 % show negative correlations with $r \leq -0.5$. However, there are distinct seasonal differences, for instance, with correlations in summer, but almost no correlation in winter regarding the same variables. The most frequent correlation exists between the saturated Brunt-Väisälä frequency N_m^2 and the lapse rates γ and Γ_m . Furthermore, as shown in Sect. 4, the SPM2D is less sensitive to N_m^2 . Thus associated correlations have less influence.

5.2 Event characteristics

30 Based on REGNIE data and the method described in Sect. 2.6, we estimate for each event within top200 the duration t_{ev} (in days), again differentiating among the seasons. The histogram of historic events and the corresponding best-fitting pdf (Fig. 12) shows that during the summer (JJA), a duration of between two and two to three days dominates with a decreasing probability

Table 3. Estimated best fitting pdfs for event duration (t_{ev}), background precipitation R_{∞} , and frontal enhancement factor c_{front} derived from REGNIE data (top box); square of saturated Brunt-Väisälä frequency N_m^2 , wind direction β , horizontal wind speed U , water vapor scale height H_w , actual lapse rate γ , saturated moist adiabatic lapse rate Γ_m , and condensation rate $\rho_{S_{ref}}$ derived from sounding data (bottom box); for the pdf aconyms: see Table 1.

model parameter	MAM	JJA	SON	DJF
t_{ev}	GEV	GEV	BSD	NkD
R_{∞}	WbD	WbD	WbD	WbD
c_{front}	LND	GmD	LND	ND
N_m^2	GEV	GbD	GEV	GEV
β	GEV	GEV	GEV	SD
U	HND	IGD	HND	GEV
γ	GEV	GEV	IGD	IGD
Γ_m	GEV	IGD	IGD	GEV
H_w	GEV	GbD	GEV	LD
$\rho_{S_{ref}}$	WbD	GEV	WbD	WbD

toward longer periods. In the winter (DJF), the distribution is generally shifted to longer events, whereas the probability for single-day events remains roughly unchanged. The maximum of 15 days in DJF represents the longest duration of top200. Whereas the estimated pdf for the summer (GEV) has a sharper maximum and a stronger decrease for $t_{ev} > 3$, the pdf found to best fit the duration in the winter (NkD) shows a broader range of possible durations. Note ~~-, however,~~ that the histogram in the winter shows a large scattering with irregular peaks, making an adjustment to a pdf very problematic. For ~~the~~ spring and autumn, the results are comparable to those of ~~the~~ winter and summer ~~respectively.~~, respectively.

Concerning background precipitation R_{∞} , totals of 20–25 mm d⁻¹ are found to most likely occur ~~with~~ within a range of 3–37 mm d⁻¹ in ~~the~~ winter, 3–50 mm d⁻¹ in ~~the~~ summer, and 0–50 mm d⁻¹ during the other two seasons (not shown). For all seasons, the Weibull distribution (WbD) is most appropriate. For frontal factor c_{front} , we obtain a log-normal distribution (LND) for ~~the~~ spring and fall, a normal pdf (ND) for the winter, and a Gamma pdf (GmD) for the summer. All pdfs have their maximums around 0.7 to 0.8 with a range from 0.4 to 1.4 for most of the seasons (not shown). The gamma distribution in ~~the~~ fall has a sharp ascent and a slower descent toward higher values (maximum of around 1.6).

5.3 Atmospheric parameters

As described in Sect. 2, orographic precipitation in the SPM2D depends on ~~the~~ seven atmospheric parameters (cf. Table 3). An overview of the range of all parameters is shown as box plots in Fig. 13. In most cases, the atmosphere was slightly stably stratified as represented by positive values of the squared Brunt-Väisälä frequency N_m^2 affecting the wave propagation. During ~~the~~ summer, the distribution is shifted toward negative values (= unstable; recall that negative values are set to $N_m = 0.0003 \text{ s}^{-1}$),

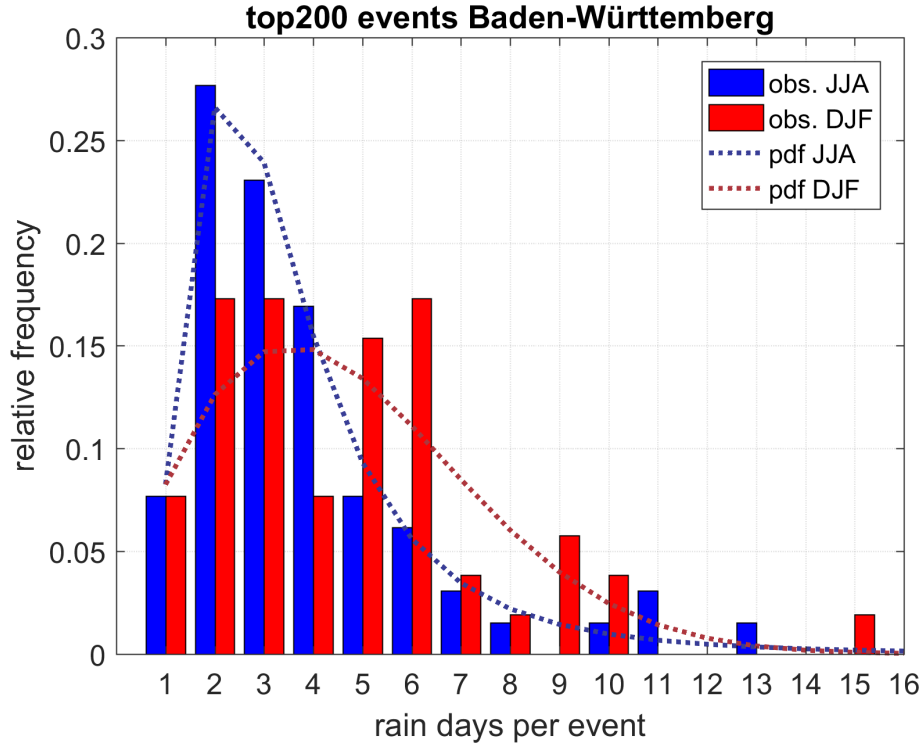


Figure 12. Histogram of top200 event duration for Baden-Württemberg according to REGNIE (bars), and estimated best fitting pdfs (dotted lines) for the summer (blue) and the winter (red).

whereas in ~~the~~ winter, there are almost entirely positive values. Wind direction β , decisive for the spatial distribution of precipitation around the mountains, ~~for example, the distribution of enhanced and reduced precipitation,~~ shows pronounced seasonal differences. More than 90 % of the top200 winter events have southwesterly to northwesterly winds (240° – 300°), with other
5 directions hardly observed. The reason is that northerly flows are usually associated with low temperatures and thus low humidity during the winter and do not have the potential for heavy precipitation. In ~~the~~ summer, the wind direction that occurred most frequently is between 240° and 300° as well. However, all other directions have been observed as well.

Horizontal wind speed U is high, especially during ~~the~~ winter, where reduced moisture is compensated by high velocity to obtain substantial horizontal incoming moisture flow. Median values are 5 and 20 m s^{-1} during ~~the~~ summer and winter
10 respectively. Flow parameters related to humidity (H_w , $\rho_{S_{ref}}$) conversely show higher values in ~~the~~ summer, where Γ_m is reduced due to the release of latent heat. Observed vertical temperature gradients γ show similar medians and interquartile ranges with a broader distribution in ~~the~~ winter.

~~In the histograms of N_m^2 for the top200 events (Fig. ??, left), distinct seasonal differences as already discussed can be identified. For both seasons, the pdf with the best fit is a GEV (special case of Gumbel in summer), yielding a longer tail to the right in the winter and a longer left tail in the summer. Seasonal differences are also well pronounced for wind direction β~~

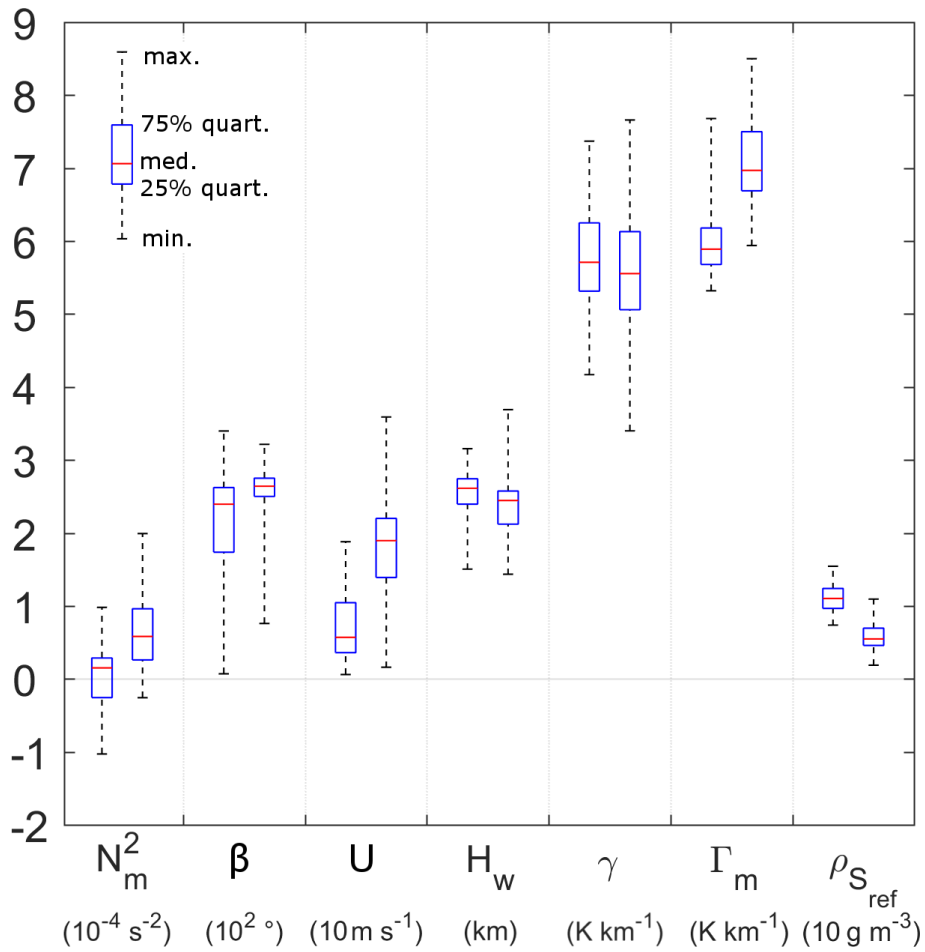


Figure 13. Atmospheric parameters required for the SPM2D derived from radiosounding observations at Stuttgart for top200 events with mean, interquartile distance, minimum, and maximum values; the left box-whisker of each pair represents the summer, the right one represents the winter season. The units for each variable are given in the brackets below the variable names.

(Fig. ??, right). Whereas during the winter time directions outside of 210° and 320° can be neglected, the distribution during the summer shows several irregularities, making the adjustment of the distribution function difficult. However, it seems to be plausible to apply a GEV distribution in the summer and the Stable distribution (SD) in the winter.

5 6 Stochastic event set and model validation

Overall, a total number of $n_E = 10,000$ events (approx. 31,500 days) have been simulated with the SPM2D, hereafter referred to as the SPM10k. For the evaluation with REGNIE data the rSPM part of this event set is referred to as rSPM10k in the following section. For the validation of the SPM2D, we quantified statistical values, such as return periods, probabilities, or

percentiles ~~and evaluate them with observations (REGNIE), CCLM simulations and the rSPM results. Note that the main reference is the REGNIE top200 event set.~~

5 Spatial 24-hour mean values for the area of Baden-Württemberg range between 1.2 ~~mm~~ and 79.7 mm in ~~the~~-SPM2D, ~~and~~
1.3 to 97.0 mm in rSPM, whereas the maximum for top200 is only 49.6 mm. In total, 128 events (~~or~~-0.4 %) of ~~the~~-SPM10k
or 724 (2.1 %) of rSPM10k yield higher spatial precipitation amounts ~~than the maximum of top200. The CCLM simulations~~
~~range between 1.8 and 37.6 mm.~~

Both median and 90th-percentile (p90) precipitation fields of top200 events and the SPM10k agree well concerning the
spatial distribution as well as the precipitation amounts (Fig. 14 Figs. 14 and 15). Significant orographic structures in the
10 precipitation fields over the Black Forest and Swabian Jura are clearly visible in ~~both~~-all data sets. ~~The areal rainfall of the~~
~~SPM10k median field differs only about 3.3% from top200, whereas that of the p90 field is about 6.5% smaller. Maximum~~
~~values in the SPM10k are about 7% higher for the median field and approximately 1% smaller for the p90 field.~~ Note that
the more detailed structure of REGNIE data results from the regionalization method and its strong dependency on orography
and should not be over-interpreted. Larger spatial differences mainly appear in the northern parts of Baden-Württemberg (the
15 Northern Rhine Valley and northeastern rolling hills) for both the median and the p90 field, ~~whereas~~-whereat for the latter,
differences also arise in an additional area northeast and southwest of Stuttgart. Nevertheless, all differences are small in the
order of a few percent. ~~The rSPM shows an overestimation of precipitation especially over mountainous terrain, whereas the~~
~~CCLM simulates overall less precipitation for the median. For the p90 field, major differences appear especially in low lands.~~

~~The areal rainfall of the SPM10k median field differs only about 3.3 % from top200, whereas that of the rSPM10k is about~~
20 ~~22.1 % higher. The spatial mean precipitation of the CCLM reanalysis is barely half of REGNIE, which might be a result of~~
~~the reduced sample size. The maximum values at any grid point for the median field are about 7 % higher in the SPM10k~~
~~compared to top200, and about 34 % higher in the rSPM10k, whereas the CCLM maximum ist about 44 % smaller. The areal~~
~~rainfall for the p90 field is about 6.5 % smaller in SPM10k, and about 14 % higher in rSPM10k, but about 22 % smaller in~~
~~CCLM. The maximum values at any grid point for the p90 field is approximately 1 % smaller in SPM10k, and about 22 %~~
25 ~~higher in rSPM10k and 13 % higher in CCLM.~~

Comparing precipitation amounts for other percentiles, for example, between the 16th and 99th percentiles (Fig. 16 a), the
differences between REGNIE and the SPM2D are very small for the spatial mean values and the maximum precipitation at any
grid point in the model domain. The differences become considerable only for the 95th percentile ~~or~~-and above. The SPM2D
tends to overestimate lower precipitation amounts because the minimum values at any grid point are higher in the model than
30 in the observations and invert for the 99th percentile only. ~~In contrast, the differences between the rSPM and REGNIE are~~
~~considerably larger for maxima, minima and spatial means throughout every percentile. The CCLM reanalysis has a negative~~
~~deviation for minimum and spatial mean precipitation in all percentiles, whereas for the maximum values there is a marked~~
~~underestimation for lower percentiles and an overestimation at higher percentiles.~~

At small percentiles, or for small precipitation amounts, respectively, QIs, such as correlation coefficient r , skill score S ,
35 and normalized standard deviation $\hat{\sigma}_f$, have low values due to the overestimation of the SPM2D (Fig. 16 b). The highest
skill is reached around the 90th percentile with a slight decrease for higher values, which can be the result of the increasing

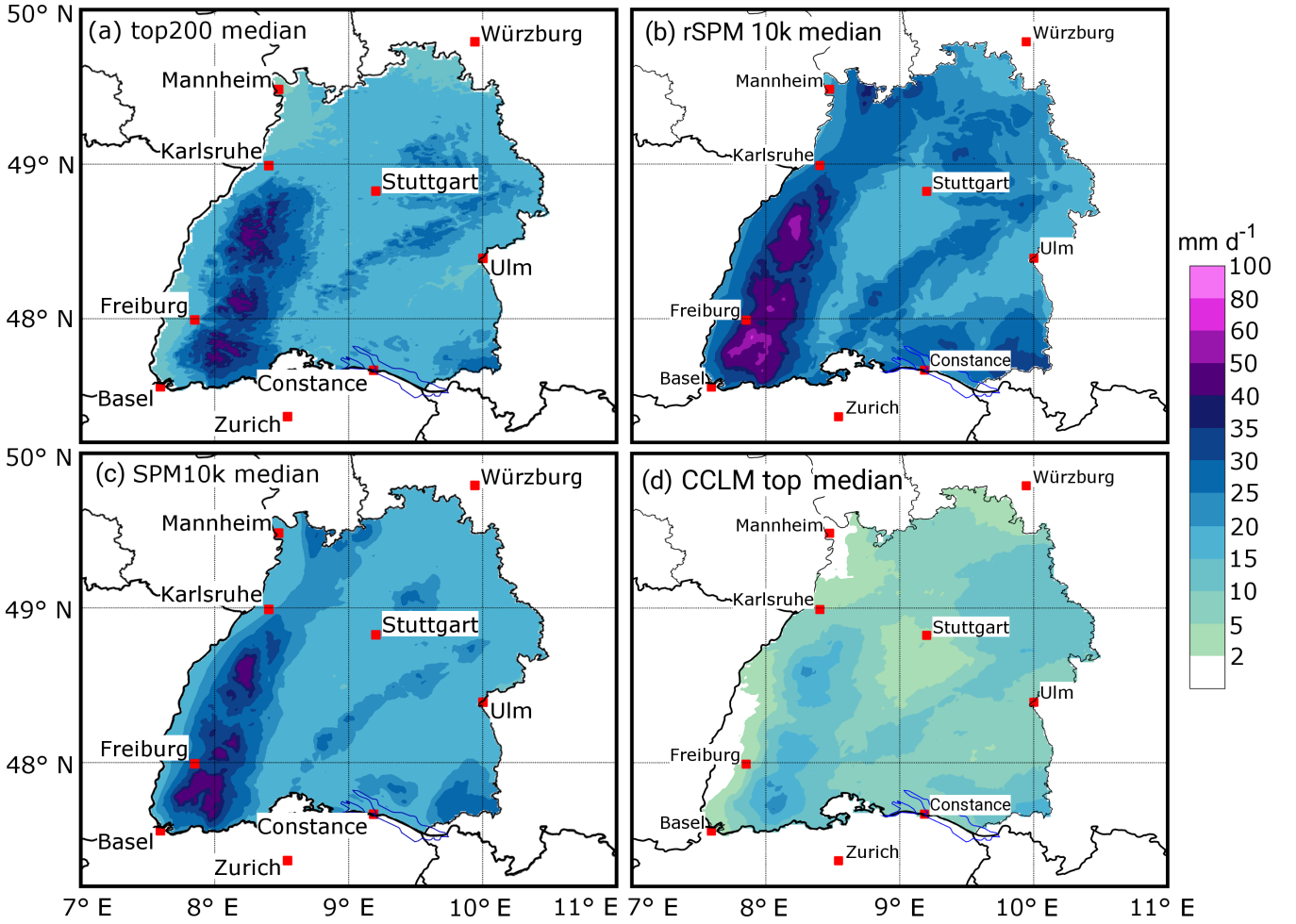


Figure 14. Precipitation fields for the median of (top) and the 90th percentile (p90; bottom) of top200 (REGNIE) events, (left column) the rSPM10k, and (c) the SPM10k, and (right column) the CCLM simulations.

uncertainties of the observations. Nevertheless, a skill score of around or above 0.8 confirms the reliability of the simulations. Note that the QIs describe the performance of the SPM2D compared to REGNIE solely. In the following we concentrate our analysis on SPM2D and REGNIE.

- 5 To estimate precipitation distributions for specific return periods, we fit a Gumbel distribution (Wilks, 2006) to the annual maximum series of both REGNIE and the SPM10k. Because As it is not possible to estimate the time period and a corresponding annual maximum series for the stochastic event set, we count the number of stochastic values exceeding the 99th percentile of observations n_{p99} and normalize it by the probability of occurrence p_{99} , producing giving the new time period T_{SPM} :

$$T_{SPM} = \frac{n_{p99}}{p_{99}}. \quad (13)$$

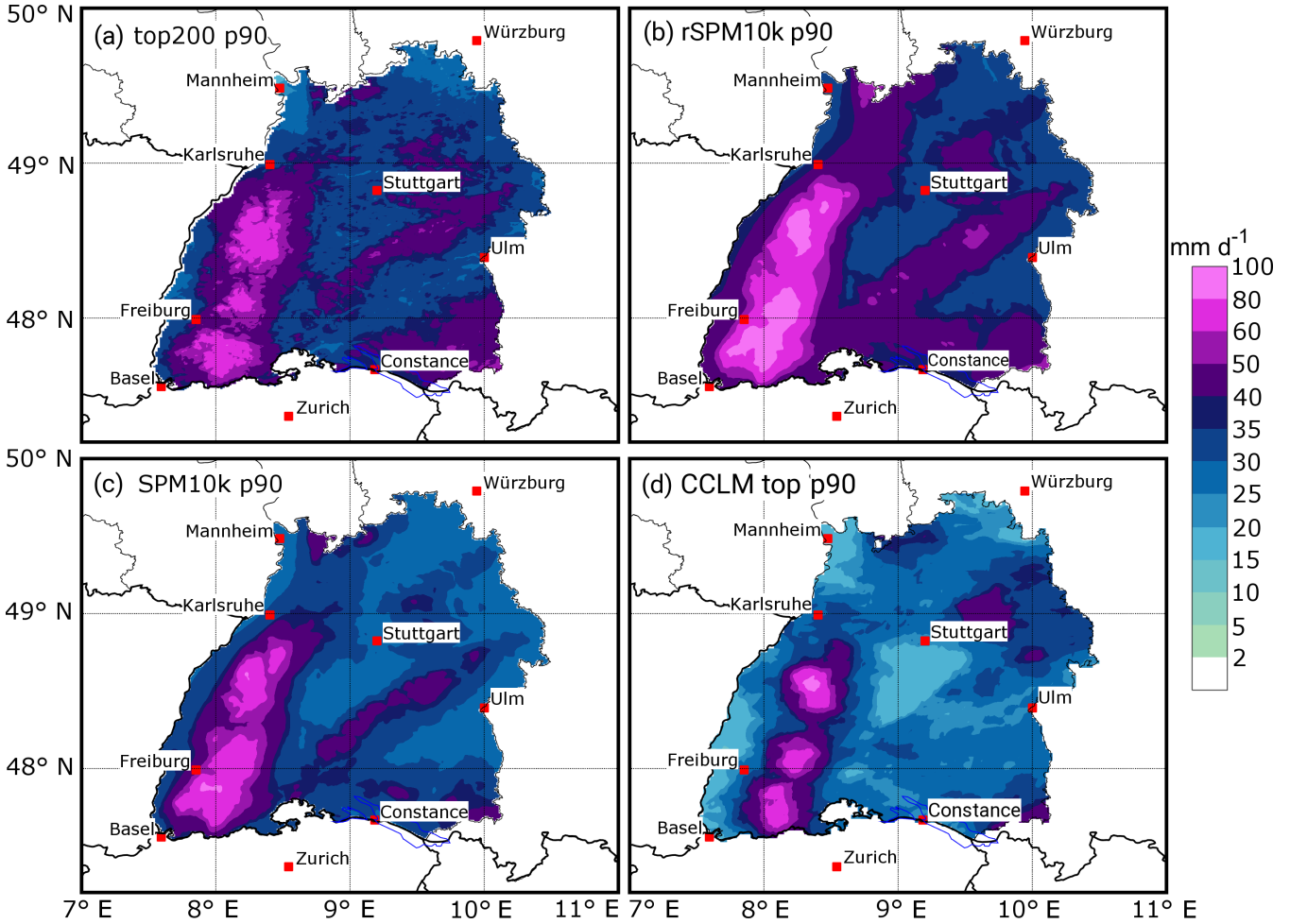


Figure 15. [Precipitation fields for the 90th percentile \(p90\) of \(a\) the top200 \(REGNIE\) events, \(b\) the rSPM10k, \(c\) the SPM10k, and \(d\) the CCLM simulations.](#)

After sorting the SPM10k in descending order, we take the first $n_T = T_{\text{SPM}}$ values as the annual series of the SPM10k and estimate a [new](#) Gumbel distribution. Using [the distribution parameters these distributions](#), we obtain precipitation values for specific return periods for both the observations and the SPM10k. This method is applied to the spatial mean values of different areas and for every single grid point.

For a 10-year return period, the SPM10k shows only small deviations from REGNIE of less than $\pm 10 \pm 10\%$ over almost the entire area of Baden-Württemberg, with a small area of overestimation in the Southern Black Forest (Fig. 17 a). The areal mean difference is only 0.6%. In the case of $T = 200$ yrs (Fig. 17 b), the overestimation in the Southern Black Forest remains with almost the same relative discrepancy. For this return period, the SPM10k tends to underestimate precipitation, especially in the northern part of Baden-Württemberg and in the southeast around Lake Constance. Nevertheless, the deviations for most

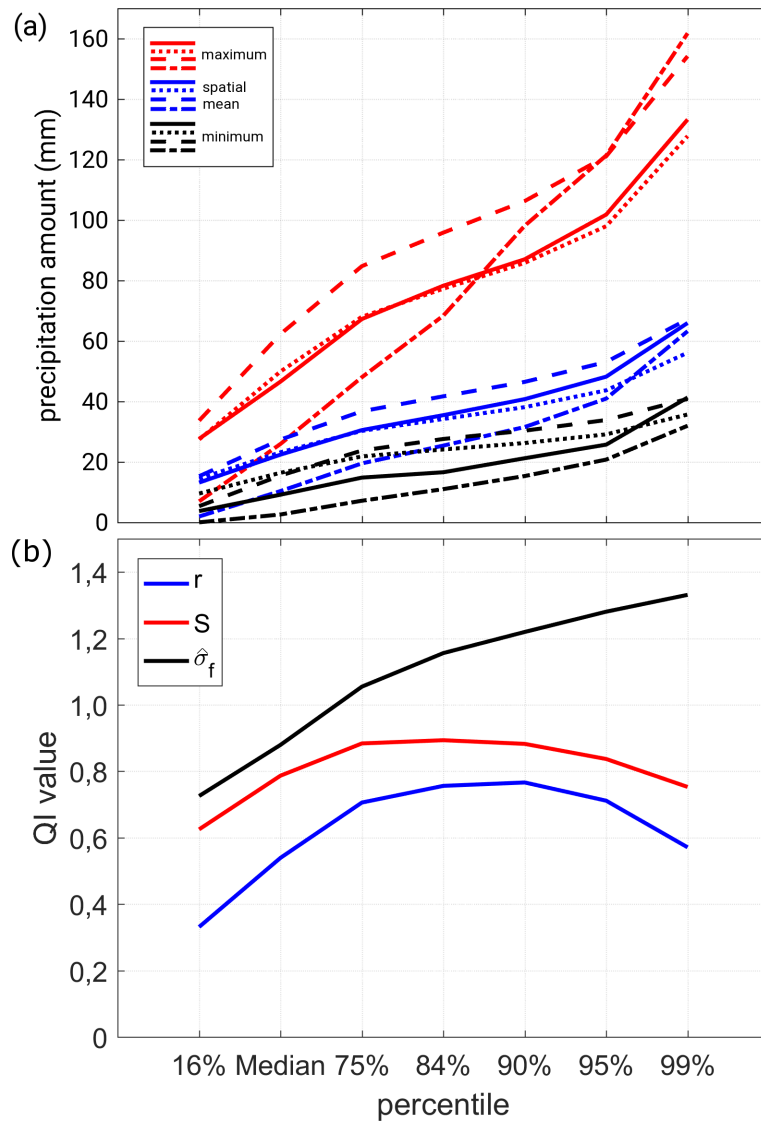


Figure 16. Comparison of (a) the maximum (red), the minimum (black), and the spatial mean precipitation (blue) of REGNIE and (solid line), the SPM2D (dotted line), the rSPM (dashed line) and CCLM simulations (dot-dashed line), and (b) quality indices (QI) r , S , and $\hat{\sigma}_f$ for different percentiles of the SPM2D compared to REGNIE.

of the grid points are between $\pm 20 \pm 20\%$, and the areal mean difference is about -10% . Taking into account the strongly increasing uncertainties of the observed values for higher return periods, especially for $T > 100$ years, this is still a reasonable result.

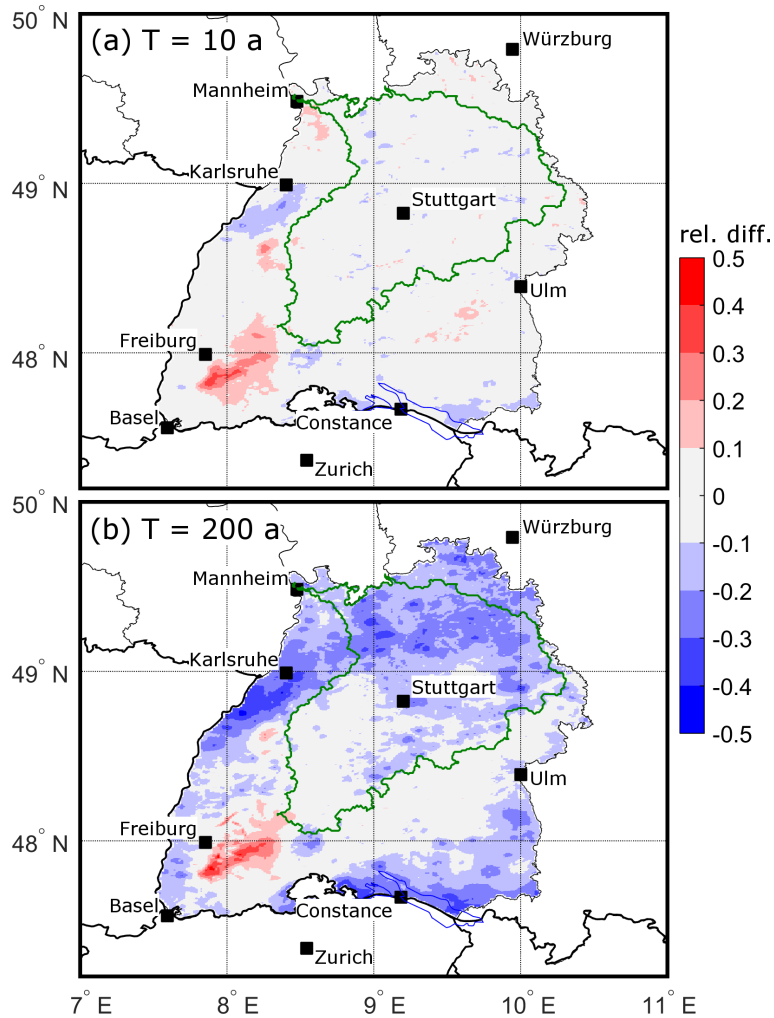


Figure 17. Relative difference of the precipitation amounts for (a) a return period of $T = 10$ years, and (b) $T = 200$ years, according to a Gumbel distribution fitted to the observations (top200) and the SPM10k (see text for further explanation). The Neckar catchment is shown as green contour.

On the level of the major river catchments, the differences ~~also are small~~ are small, too. For the Neckar catchment, for example (see Fig. 17), which covers about 38% of Baden-Württemberg, the spatial mean deviation is about -0.5% in the case of $T = 10$ yrs and -12.7% for the 200-year return period. Even for the catchments containing the area of overestimation in the Southern Black Forest (Upper Rhine between Basel and Mannheim, and High Rhine between Constance and Basel), the spatial mean deviations are between $+1$ and $+4\%$ for $T = 10$ yrs and between -2 and -10% for $T = 200$ yrs respectively.

Single grid point deviations and the ensuing spatial mean values as described above are sensitive to local conditions and uncertainties in both REGNIE and SPM10k data. Hence, we evaluate the model in a similar way by calculating the spatial mean

precipitation first and then fitting a Gumbel distribution to the spatial means in a second step. For the plotting, return period T_k of each element x_k of the annual maximum series with length T_{max} is given by $T_k = T_{max} \cdot rk(x_k)$ with the rank $rk(x_k)$ of element x_k (annual series sorted in descending order). The first element (highest value) of an annual series of, for example, 100 years therefore has a return period of $T_1 = 100$ yrs, the second $T_2 = 50$ yrs, and so on. The values of T_k were adjusted using the plotting position method of Cunnane (1978).

Again, the difference between the simulated and observed spatial mean values of daily precipitation for the whole of Baden-Württemberg is small, with slightly lower values from the simulations (Fig. 18 a). The distribution of the SPM10k is very close and almost parallel to the estimated observed Gumbel distribution and mostly in-between or close to within the 95 % confidence interval (CI95) estimated with the formula of Dyek (1980) Maity (2018). Considerable differences between the SPM10k and REGNIE arise only for return periods of $T = 1000$ yrs and above but are still small. For the Neckar catchment, the simulation results agree well with the observed distribution for return periods up to approximately 300 years (Fig. 18 b). For higher return periods, the differences increase but are still inside or around the CI95. Similar results can be found for other river catchments. Note again that for such high return values, the statistical uncertainty of the observed distribution also increases significantly.

7 Summary and Conclusions

We have presented a novel method for estimating the statistics of total rainfall based on a stochastic model approach (SPM2D). Total precipitation at any each grid point is calculated from the linear superposition of four different parts: orographic precipitation, synoptic background precipitation, frontal precipitation and embedded convection precipitation from convection embedded into stratiform clouds. The linear theory of orographic precipitation according to Smith and Barstad (2004), which represents the core of the SPM2D, has been modified by using three different calibration parameters to minimize the weaknesses found in previous studies (e.g., Barstad and Smith, 2005; Kunz, 2011) and to adjust the model to the specific conditions of the investigation area. We such as the overestimation of wave dynamics and, thus, resulting precipitation and evaporation (e.g., Barstad and Smith, 2005; Kunz, 2011). For cross-validation, we calibrated and adjusted the SPM2D to a historic event set of heavy rainfall events (top200). Using training data. By adjusting appropriate probability density functions (pdfs) for all required model parameters, we simulated 10,000 independent stochastic precipitation events and compared the results with observations (validation data). The results were compared with observations and reanalysis data using different percentiles or and return periods.

The focus of the presented investigations was on the Federal State of Baden-Württemberg in Southwest Germany with the striking low-mountain ranges of Black Forest and Swabian Jura. The following main conclusions can be drawn:

- The results illustrate the capability of the SPM2D to both simulate has a high skill to simulate both historic and stochastic events with realistic spatial distribution and magnitude despite its simple approach of using just seven atmospheric variables for precipitation calculation heavy rainfall events. The simulated spatial distributions and magnitudes are reliable despite the simplified approach of the model initialized by a set of atmospheric variables obtained from radio-soundings. The differences between the SPM2D and REGNIE are small with deviations of less than 10 %. Local

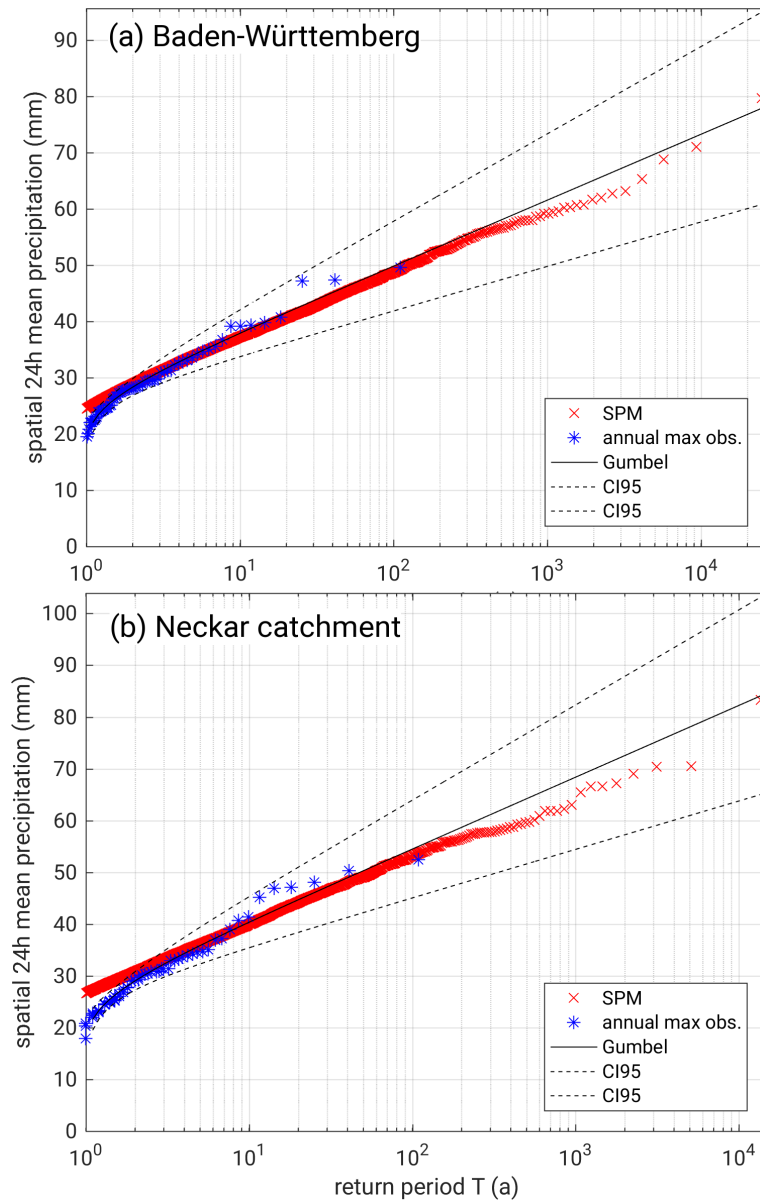


Figure 18. Daily rainfall totals (areal mean) as a function of return period T based on the annual maximum series of observations (REGNIE, blue), the corresponding Gumbel distribution including the 95 % confidence intervals (black), and the annual SPM10k series (red) for (a) the Federal State of Baden-Württemberg, and (b) the Neckar catchment.

differences ~~may be the result of an inhomogeneous~~, however, ~~may also be traced back to uncertainties in REGNIE observations, mainly because of prevailing inhomogeneities in the spatial distribution of rain gauges, which leads to discrepancies in the interpolated REGNIE fields. The interpolation method used for REGNIE furthermore~~

~~overemphasizes the orographic influence on the precipitation distribution whereby more uncertainties emerge especially over mountainous terrain.~~

- 5 – ~~The comparison of the SPM2D with the reduced stochastic model rSPM demonstrates the need to additionally consider precipitation related to frontal systems and embedded convection. The SPM2D with simplified parameterizations for these parts even yields more reliable precipitation fields for a historic event set compared to the sophisticated high-resolution NWP model CCLM.~~
- 10 – ~~The solution of the model equations in the Fourier space using a fast Fourier transform algorithm allows for simulations in the Fourier space by an FFT allows for the simulation of a large number of events with less temporal effort. Furthermore, wave dynamics are directly implemented, and to run the model in stochastic mode.~~
- 15 – ~~The linear approach for orographic precipitation worked quite well during calibration to historic events (top200). The newly added amounts for frontal precipitation and embedded convection as well as the implemented model parameters afford even more plausible realizations on a physical basis: f_{C_w} decreases the sensitivity of orographic precipitation on multiple ascents; f_{dry} reduces the underestimation of lee-side precipitation due to evaporation; and c_{oro} takes into account the extent of the model domain has to be limited to ensure the validity of the assumption of an entirely saturated atmosphere at any time.~~ spatially homogeneous distributed atmospheric conditions and synoptic forcing. This allows, for instance, for the usage of a vertical profile from a single radiosounding station (or model data).
- 20 – ~~The presented stochastic approach is easily applicable to other investigation areas. Prerequisite information of atmospheric variables~~ Atmospheric variables for the initialization of the model can be estimated based on radiosoundings, either from radiosoundings as within this study, or based on reanalysis or forecast data of numerical weather or climate or using reanalysis or data from NWP models. Therefore, it can be used for precipitation simulations in areas with less or even no applied to any region of the world with similar precipitation characteristics even if there is only a limited number of ground-based observations available.
- 25 As shown in ~~a case our~~ study, the SPM2D is sensitive to perturbations of ambient conditions, ~~and therefore,~~ Therefore, high-quality input data, especially of the atmospheric parameters, are essential. ~~Both radiosoundings or numerical model outputs may not correctly represent the undisturbed conditions upstream of the investigation area due to, for example, an inconvenient location of the launching station of the radiosondes or measurement errors, which leads to hardly quantifiable uncertainties in the SPM2D~~ On the other hand, the sensitivities of precipitation and rmse to changing input parameters is limited in a range of around $\pm 10\%$ of the original values, which is usually within the range of uncertainty. Using data of only one sounding station turned out to be sufficient to achieve reliable heavy rainfall fields. As shown by (Kunz, 2011), the differences to another upstream sounding station (Nancy in France) are small, at least in the mean. This, however, applies only for widespread precipitation with durations over several hours to days, which is the focus of our study. Intermittent or even mainly convectively-driven events cannot be reliably reproduced by our model.
- 30

The input parameters can be considered as independent, as just a few cases revealed higher correlation. The sensitivity of the model for these parameters, however, turned out to be weak. Additionally, the correlation coefficients between the model input parameters vary among the seasons.

5 To transfer the method to another investigation area, just a few steps are necessary: first a proper sample of historical heavy rainfall events. In the next step, the statistics (pdfs) of the prevailing ambient conditions, background precipitation, and duration for the event set have to be calculated. Finally, the reduced SPM (rSPM) has to be calibrated by determining appropriate values for the free model tuning parameters.

The presented SPM2D is part of ~~a~~ the project FLORIS (Flood Risk), which represents a novel risk assessment methodology ~~that estimates the flood risk for a local direct insurer~~ for an entire domain and not only for single catchments applied in the insurance industry. Within the framework of this project, the SPM2D ~~is used for two more~~ was applied to other federal states in ~~Central Germany with the quality of the results resembling those presented for Baden-Württemberg in this study. The precipitation fields simulated with the SPM2D~~ central Germany. The modeled precipitation fields are used as input data for hydrological ~~simulations with the aim of the flood risk estimation of a one-in-200-year event and the corresponding probable~~ maximum loss (PML200), as it is mandatory by law for the insurance industry to maintain capital stock for such an event.

15 Besides the PML200 for insurance companies, the proper statistics of extreme events are useful for multifarious issues in different fields of water management, such as ~~and~~ hydraulic simulations, from which the flood ~~protection with dams or retention areas, or forecast scenarios~~ risk can be estimated, for example for a one-in-200-years event required according to the insurance regulation of Solvency II. However, the results of the SPM2D basically can be used for several different applications such as ~~water management or the design of flood protection measures.~~

8 Data availability

The REGNIE data used in this paper are freely available for research and can be requested at the DWD (doi:10.1127/0941-2948/2013/0436); The sounding data are freely available from the Integrated Global Radiosonde Archive (<https://www.ncdc.noaa.gov/data-access/weather-balloon/integrated-global-radiosonde-archive>). The required orographic data set ~~(doi:10.1080/13658810601169899) can be downloaded~~ obtained from <http://srtm.csi.cgiar.org/>.

Competing interests. The authors declare that they have no conflict of interest.

Acknowledgements. The authors thank a local insurance company for funding the project. We also would like to thank the German Weather Service (DWD) and the Integrated Global Radiosonde Archive (IGRA) for providing different observational data sets and CGIAR-CSI for the orographic data. Special thanks go to James Daniell, Andreas Kron and Simon Hoellering from KIT for constructive discussions within the project and for valuable suggestions during the model development. We acknowledge support by Deutsche Forschungsgemeinschaft (DFG)

and open access publishing fund of Karlsruhe Institute of Technology (KIT). We are grateful to the constructive comments and suggestions of three anonymous reviewers that helped to improve the quality of this paper.

References

- Barstad, I. and Caroletti, G. N.: Orographic precipitation across an island in southern Norway: model evaluation of time-step precipitation, *Q. J. R. Meteorol. Soc.*, 139, 1555–1565, 2013.
- Barstad, I. and Smith, R. B.: Evaluation of an Orographic Precipitation Model, *J. Hydrometeorol.*, 6, 85–99, 2005.
- Basist, A., Bell, G. D., and Meentmeyer, V.: Statistical relationships between topography and precipitation patterns, *J. Climate*, 7, 1305–1315,
5 1994.
- Bergeron, T.: On the physics of fronts, *Bull. Am. Meteorol. Soc.*, 18, 265–275, 1937.
- Browning, K. A., Pardoe, C. W., and Hill, F. F.: The nature of orographic rain at wintertime cold fronts, *Q. J. R. Meteorol. Soc.*, 101, 333–352,
1975.
- Cannon, D. J., Kirshbaum, D. J., and Gray, S. L.: Under what conditions does embedded convection enhance orographic precipitation?, *Q. J.
10 R. Meteorol. Soc.*, 138, 391–406, 2012.
- Caroletti, G. N. and Barstad, I.: An assessment of future extreme precipitation in western Norway using a linear model, *Hydrol. Earth Syst.
Sci.*, 14, 2329–2341, 2010.
- Crochet, P., Jóhannesson, T., Jónsson, T., Sigurdsson, O., Björnsson, H., Pálsson, F., and Barstad, I.: Estimating the spatial distribution of
precipitation in Iceland using a linear model of orographic precipitation, *J. Hydrometeorol.*, 8, 1285–1306, 2007.
- 15 Cross, D., Onof, C., Winter, H., and Bernardara, P.: Censored rainfall modelling for estimation of fine-scale extremes, *Hydrol. Earth Syst.
Sci. Discuss.*, <https://doi.org/10.5194/hess-2017-437>, 2017.
- Cunnane, C.: Unbiased plotting positions – a review, *J. Hydrol.*, 37, 205–222, 1978.
- Drogue, G., Humbert, J., Deraisme, J., Mahr, N., and Freslon, N.: A statistical-topographic model using an omnidirectional parameterization
of the relief for mapping orographic rainfall, *Int. J. Climatol.*, 22, 599–613, <https://doi.org/10.1002/joc.671>, 2002.
- 20 Duckstein, L., Bárdossy, A., and Bogárdi, I.: Linkage between the occurrence of daily atmospheric circulation patterns and floods: an Arizona
case study, *J. Hydrol.*, 143, 413–428, 1993.
- Durrán, D. R. and Klemp, J. B.: On the effects of moisture on the Brunt-Väisälä frequency, *J. Atmos. Sci.*, 39, 2152–2158, 1982.
- Durre, I., Vose, R. S., and Wuertz, D. B.: Overview of the integrated global radiosonde archive, *J. Climate*, 115(1), 53–68, 2006.
- Dyck, S.: *Angewandte Hydrologie, Teil 1: Berechnung und Regelung des Durchflusses der Flüsse.*, 2 edn., 1980.
- 25 Eliassen, A.: On the vertical circulation in frontal zones, *Geophys. Publ.*, 24, 147–160, 1962.
- Fluck, E.: Hail statistics for European countries, Phd thesis, Institute of Meteorology and Climate Research (IMK), Karlsruhe Institute of
Technologie (KIT), Karlsruhe, Germany, <https://doi.org/10.5445/IR/1000080663>, 2018.
- Freedman, D. and Diaconis, P.: On the histogram as a density estimator: L2 theory, *Zeitschrift für Wahrscheinlichkeitstheorie und Verwandte
Gebiete*, 57, 453–476, <https://doi.org/10.1007/BF01025868>, 1981.
- 30 Fuhrer, O. and Schär, C.: Embedded cellular convection in moist flow past topography, *J. Atmos. Sci.*, 62, 2810–2828, 2005.
- Furrer, E. M. and Katz, R. W.: Generalized linear modeling approach to stochastic weather generators, *Clim. Res.*, 34, 129–144, 2007.
- Goovaerts, P.: Geostatistical approaches for incorporating elevation into the spatial interpolation of rainfall, *J. Hydrol.*, 228, 113–129, 2000.
- Handwerker, J.: Cell tracking with TRACE3D - a new algorithm, *Atmos. Res.*, 61, 15–34, 2002.
- Houze, R. A. and Hobbs, P. V.: Organization and Structure of Precipitation cloud systems, *Adv. Geophys.*, 24, 225–315, 1982.
- 35 Jiang, Q. and Smith, R. B.: Cloud timescales and orographic precipitation, *J. Atmos. Sci.*, 60, 1543–1559, 2003.
- Källberg, P., Simmons, A., Uppala, S., and Fuentes, M.: The ERA-40 archive. [Revised October 2007], Shinfield Park, Reading, 2004.

- Kienzler, S., Pech, I., Kreibich, H., Müller, M., and Thielen, A. H.: After the extreme flood in 2002: changes in preparedness, response and recovery of flood-affected residents in Germany between 2005 and 2011, *Nat. Hazards Earth Syst. Sci.*, 15, 505–526, 2015.
- Kirshbaum, D. J. and Durran, D. R.: Factors governing cellular convection in orographic precipitation, *J. Atmos. Sci.*, 61, 682–698, 2004.
- Kirshbaum, D. J. and Smith, R. B.: Temperature and moist-stability effects on midlatitude orographic precipitation, *Q. J. R. Meteorol. Soc.*, 134, 1183–1199, <https://doi.org/10.1002/qj.274>, 2008.
- 5 Koutsoyiannis, D., Kozonis, D., and Manetas, A.: A mathematical framework for studying rainfall intensity-duration-frequency relationships, *J. Hydrol.*, 206, 118–135, 1998.
- Kunz, M.: Characteristics of Large-Scale Orographic Precipitation in a Linear Perspective, *J. Hydrometeorol.*, 12, 27–44, 2011.
- Kunz, M. and Wassermann, S.: Moist dynamics and sensitivity of orographic precipitation to changing ambient conditions in an idealised perspective, *Meteorol. Z.*, 20, 199–215, 2011.
- 10 Lalas, D. P. and Einaudi, F.: On the stability of a moist atmosphere in the presence of a background wind, *J. Atmos. Sci.*, 30, 795–800, 1973.
- Laube, N.: personal correspondence, Phd thesis, Institute of Meteorology and Climate Research (IMK), Karlsruhe Institute of Technology (KIT), Karlsruhe, Germany, 2018.
- Maity, R.: *Statistical Methods in Hydrology and Hydroclimatology*, Springer Nature Singapore Pte Ltd., <https://doi.org/10.1007/978-981-10-8779-0>, 2018.
- 15 Mardia, K. V. and Zemroch, P. J.: Algorithm AS 86: The Von Mises Distribution Function, *Journal of the Royal Statistical Society. Series C (Applied Statistics)*, 24, 268–272, 1975.
- Mason, B.: *The physics of clouds*, Oxford University Press, 671 pp., 1971.
- MATLAB: MATLAB and Statistics Toolbox Release 2016b, (version 9.1), The MathWorks Inc., Natick, Massachusetts, USA, <http://de.mathworks.com/help/>, last visited 10 August 2017, 2016.
- 20 Mohr, S. and Kunz, M.: Recent trends and variabilities of convective parameters relevant for hail events in Germany and Europe, *Atmos. Res.*, 123, 211–228, 2013.
- MunichRe: NatCatSERVICE, natcatservice.munichre.com/, accessed: 28 Sept 2017, 2017.
- Neykov, N. M., Neytchev, P. N., and Zucchini, W.: Stochastic daily precipitation model with a heavy-tailed component, *Nat. Hazards Earth Syst. Sci.*, 14, 2321–2335, <https://doi.org/10.5194/nhess-14-2321-2014>, 2014.
- 25 Palutikov, J. P., Brabson, B., Lister, D. H., and Adcock, S. T.: A review of methods to calculate extreme wind speeds, *Meteorol. Appl.*, 6, 119–132, 1999.
- Petrow, T., Zimmer, J., and Merz, B.: Changes in the flood hazard in Germany through changing frequency and persistence of circulation patterns, *Nat. Hazards Earth Syst. Sci.*, 9, 1409, 2009.
- Piper, D., Kunz, M., Ehmele, F., Mohr, S., Mühr, B., Kron, A., and Daniell, J.: Exceptional sequence of severe thunderstorms and related flash floods in May and June 2016 in Germany-Part 1: Meteorological background, *Nat. Hazards Earth Syst. Sci.*, 16, 2835, 2016.
- 30 Rauthe, M., Steiner, H., Riediger, U., A., M., and Gratzki, A.: A Central European precipitation climatology - Part I: Generation and validation of a high-resolution gridded daily data set (HYRAS), *Meteorol. Z.*, 22, 235–256, 2013.
- Richardson, C. W.: Stochastic Simulation of Daily Precipitation, Temperature, and Solar Radiation, *Water Resour. Res.*, 17, 182–190, 1981.
- Rockel, B., Will, A., and Hense, A.: The regional climate model COSMO-CLM (CCLM), *Meteorol. Z.*, 17, 347–348, 2008.
- 35 Schröter, K., Kunz, M., Elmer, F., Mühr, B., and Merz, B.: What made the June 2013 flood in Germany an exceptional event? A hydro-meteorological evaluation, *Hydrol. Earth Syst. Sci.*, 19, 309–327, 2015.
- Smith, R. B.: Linear theory of stratified hydrostatic flow past an isolated mountain, *Tellus*, 32, 348–364, 1980.

- Smith, R. B.: Hydrostatic airflow over mountains, *Adv. Geophys.*, 31, 1–41, 1989.
- Smith, R. B. and Barstad, I.: A Linear Theory of Orographic Precipitation, *J. Atmos. Sci.*, 61, 1377–1391, 2004.
- Spearman, C.: The Proof and Measurement of Association between Two Things, *The American Journal of Psychology*, 15, 72–101, 1904.
- Taylor, K. E.: Summarizing multiple aspects of model performance in a single diagram, *J. Geophys. Res.*, 106, 7183–7192, 2001.
- Uhlmann, S., Thielen, A. H., and Merz, B.: A consistent set of trans-basin floods in Germany between 1952-2002, *Hydrol. Earth Syst. Sci.*,
5 14, 1277, 2010.
- Wanner, H., Rickli, R., Salvisberg, E., Schmutz, C., and Schüepp, M.: Global climate change and variability and its influence on alpine climate-concepts and observations, *Theor. Appl. Climatol.*, 58, 221–243, 1997.
- Wilks, D. S.: *Statistical Methods in the Atmospheric Sciences*, vol. 91 of *International Geophysics Series*, Academic Press, San Diego, California, USA, 2nd edn., 2006.